



Published in final edited form as:

J Med Chem. 2018 February 08; 61(3): 666–680. doi:10.1021/acs.jmedchem.7b00530.

Structure-Guided Synthesis and Mechanistic Studies Reveal Sweetspots on Naphthyl Salicyl Hydrazone Scaffold as Non-Nucleosidic Competitive, Reversible Inhibitors of Human Ribonucleotide Reductase

Sarah E. Huff[‡], Faiz Ahmad Mohammed[¶], Mu Yang[‡], Prashansa Agrawal[‡], John Pink[†], Michael E. Harris[§], Chris G. Dealwis^{¶,*}, and Rajesh Viswanathan^{‡,†,*}

[†]Frank Hovorka Assistant Professor of Chemistry and Scientific Oversight Board Member – Small Molecule Drug Discovery Core, CWRU, 10900 Euclid Ave, Cleveland, OH 44106.

[‡]Department of Chemistry, Case Western Reserve University, College of Arts and Sciences, Millis Science Center: Rm 216, 2074, Adelbert Road, Cleveland, OH 44106-7078.

[¶]Department of Pharmacology, Case Western Reserve University, School of Medicine, 10900 Euclid Ave, Cleveland, OH 44106.

[§]Department of Chemistry, University of Florida, PO Box 117200, Gainesville, FL 32611.

[†]Case Comprehensive Cancer Center, Case Western Reserve University, School of Medicine, 10900 Euclid Ave, Cleveland, OH 44106.

^{*}Center for Proteomics and the Department of Chemistry, Case Western Reserve University, 10900 Euclid Ave, Cleveland, OH 44106.

Abstract

Ribonucleotide reductase (RR), an established cancer target is usually inhibited by antimetabolites which display multiple cross-reactive effects. Recently, we discovered a naphthyl salicyl acyl hydrazone-based inhibitor (NSAH or E-3a) of human RR (hRR) binding at the catalytic site (C-

*Corresponding author: Rajesh Viswanathan rajesh.viswanathan@case.edu.

ORCID*s*

Rajesh Viswanathan: 0000-0003-4107-3962

Chris G. Dealwis: 0000-0002-1686-4183

Michael E. Harris: 0000-0001-8977-4392

John J. Pink: 0000-0002-3111-5754

Prashansa Agrawal: 0000-001-6803-3261

Associated Content

Supporting Information

Molecular formula strings as SMILES entries is provided as Supporting Information file. General synthetic methods, docking poses for some inhibitors at the C-site, experimental methods for metal chelation studies, copies of spectra, enzyme assay tabulated data and dose-response curves for **3a**, **3c**, **3t** and **3w** are provided in the Supporting Information file. The Supporting Information file is available free of charge on the ACS Publications website at DOI:

Competing Financial Interests

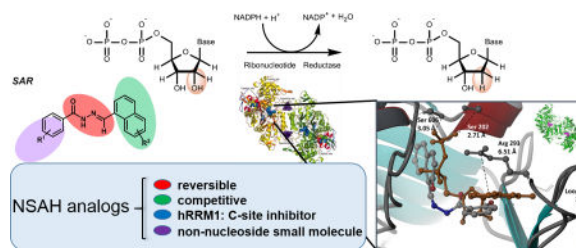
The authors declare no competing financial interests

Author Contributions

CGD, MEH and RV designed the project. SEH, FAM, JP and MY performed experiments. JP performed all cell-based experiments. RV, SEH, MEH, JP and CGD wrote the manuscript. Prashansa Agrawal contributed to collection and helped in analysis of NMR spectral data for compounds.

site) and inhibiting hRR reversibly. We herein report the synthesis and biochemical characterization of 25 distinct analogs. We designed each analog through docking to the C-site of hRR based on our 2.7 Å X-ray crystal structure (PDB ID: 5TUS). Broad tolerance to minor structural variations preserving inhibitory potency is observed. *E-3f* (82% yield) displayed an *in vitro* IC₅₀ of 5.3 ± 1.8 μM against hRR, making it the most potent in this series. Kinetic assays reveal that *E-3a*, *E-3c*, *E-3t* and *E-3w* bind and inhibit hRR through a reversible and competitive mode. Target selectivity towards the R1 subunit of hRR is established, providing a novel way of inhibition of this crucial enzyme.

Graphical Abstract



Introduction

Ribonucleotide reductase (RR) catalyzes the conversion of ribonucleoside substrates into deoxyribonucleosides (Figure 1A), the rate-limiting step in the formation of all deoxyribonucleoside 5'-triphosphates (dNTPs) as building blocks for DNA synthesis and replication.¹ Therefore, RR crucially maintains a balanced nucleotide pool in the cell. Consequently, RR has been an established target for many proliferative diseases, including cancer.² Additionally, RR is a relatively complex cellular target for anti-cancer therapeutic development due to the fact that inhibition of this critical enzyme is likely to cause cell death even in normal cells. This presents an additional layer of challenge to develop RR inhibitors that can target cancer cells selectively.

Foundational knowledge on allosteric regulation of this multi-subunit enzyme has been extensively probed through a series of studies conducted on prokaryotic and some eukaryotic RRs.¹ Mechanistic details of substrate regulation through allostery also remains a focus of ongoing investigations.³ Recent studies have provided structural insights underlying allosterically driven dNTP regulation by RR.^{1d-e, 4, 5c} Though previous studies establish the molecular details of multimerization as a basis for development of novel anticancer agents,⁵ there has been little focus on identifying non-nucleosidic, reversible and competitive inhibitors of RR.

With the exceptions of hydroxyurea, triapine, and related radical scavengers that target the R2 subunit, most small-molecule anticancer agents targeting RR belong to the antimetabolite class of antineoplastic agents (see Table S1 for a list of FDA-approved drugs). For example gemcitabine, FDA approved for treatment of breast, ovarian, non-small cell lung and pancreatic cancer, is a nucleoside analog that structurally mimics ribonucleoside diphosphate substrates.⁶ Gemcitabine inactivates the RR enzymatic machinery by covalently

and irreversibly modifying an active site nucleophilic Cys sulfhydryl moiety, causing significant abrogation of enzyme function.⁶ There is little distinction if any for the action of gemcitabine between RRs in normal cells versus RRs in cancer cells, resulting in toxic side effects in chemotherapy.⁶ Clofarabine and others inhibit hRR through a non-covalent mode; however, in general the antimetabolite class of inhibitors significantly cross react with essential nucleotide metabolic enzymes causing indiscriminate toxicity. For example, clofarabine triphosphate causes chain termination of DNA polymerase activity.⁷

Given this background, we hypothesized that reversible, non-covalent inhibitors of hRR that are non-nucleosidic may show reduced cross reactivity, and thereby reduced side effects and toxicity. In 2015, we reported an integrated approach consisting of *in silico* rapid throughput screening of small molecules, *in vitro* biochemical assays against hRR, cellular growth inhibition studies against select cancer cell lines, and X-ray crystallography to guide us with future rational design.⁸ This integrated approach afforded identification of several new classes of non-nucleosidic modulators of hRR with *in vitro* hRR inhibitory potencies in the micromolar range. Detailed X-ray crystallography revealed the binding of a phthalimide-containing class of modulators maintaining non-covalent stabilizing interactions at the hexamerization interface of hRR.^{8,9}

Subsequent to the 2015 report, we discovered a lead compound, Naphthyl Salicyl Acylhydrazone (NSAH or *E-3a*) that binds to the catalytic site (C-site) of hRRM1 (Figure 1B).¹⁰ *E-3a* demonstrated significant levels of selective cytotoxicity against multiple cancer cell lines while displaying little cytotoxicity against normal mobilized peripheral blood progenitor cells.¹⁰ This result presented us with a lead compound possessing favorable properties worthy of further exploration. In the present study we use the previously determined 2.7 Å crystal structure of this lead inhibitor (*E-3a*) in complex with hRRM1 (PDB ID: 5TUS)¹⁰ as a template for structure-based ligand optimization. We designed suitable analogs of *E-3a*, docked them to the C-site of hRR using the Schrödinger software suite, and evaluated their docking poses to predict which analogs would show increased inhibitory efficacy relative to the lead compound, *E-3a*. We then synthesized and biochemically characterized a series of twenty five analogs (*E-3a-z*) as hRR inhibitors and established preliminary structure-activity evaluations (Figure 1C). A five step, modular synthetic scheme was developed that generally afforded analogs in yields ranging between 63% and 85%, with few exceptions. *E-3f* was obtained in 82% yield and displayed an *in vitro* IC₅₀ of 5.3 ± 1.8 μM against hRR, making it the most potent in this series of analogs. Ranking of the analogs by their enzymatic IC₅₀ value reveals that the inclusion of a polar substituent in the ortho position of the salicylic moiety is critical for biological activity, while the substitution of an indole ring for a naphthalene ring showed no loss in activity. Detailed kinetics assays reveal that these inhibitors bind and inactivate hRR through a reversible and competitive mode, consistent with our recently reported finding for the lead inhibitor *E-3a*.¹⁰ Remarkably, this class of compounds are the first non-nucleosidic inhibitors of hRR displaying a competitive, reversible mode of inhibition, consistent with C-site binding.

Results

In silico modeling based upon the X-ray crystal structure of *E-3a* in complex with hRRM1 (PDB ID: 5TUS) was used to design a focused library of hydrazone-based hRR inhibitors.¹⁰ Approximately one hundred distinct analogs with unique substitution patterns surrounding the central hydrazone core were docked to the C-site, where the grid was defined as a 5 Å cube centered around the lead hydrazone ligand. Evaluation of the docking poses for interactions with residues previously established to interact with nucleoside substrates, such as Ser 202, Ser 606, Gly 246, Cys 218, Cys 429 and Ser 217, helped define a subset of twenty five analogs most likely to bind at the C-site and inhibit the enzyme. We noted the key residues involved in NDP binding in the C-site of hRR and catalysis, such as: Glu 431, Cys 429, Cys 444, Cys 218 and Asn 427. Upon comparing the close hydrogen bonding contacts between parent inhibitor (*E-3a*) at the C-site of hRR in our recent X-ray structure (PDB ID: 5TUS)¹⁰, Ser 217 and Cys 218 made relevant contacts through hydrogen bonds with *E-3a*. Cys 429 offered weaker Van der Waals contact with inhibitor *E-3a*, however it did not contribute strongly to stabilize binding to the inhibitor. The docking poses along with predicted affinities of representative candidates to the C-site of hRR, are presented in Figure 2A–F.

The library of compounds (*E-3a-z*) were docked against the S-site and A-site of hRRM1 to determine if any analogs were likely to bind to allosteric sites other than the C-site. The Schrödinger docking scores for all sites are reported in Table S3. In general, a lower score is considered favorable, with scores between 0 and -5 considered poor and scores of -10 or lower considered an indication of strong binding interactions. The docking scores for the C-site ranged from -6.26 to -7.76, indicating favorable interactions between the ligands and C-site residues. The scores for the A-site ranged from -2.99 to -5.23, with only two compounds reporting a score below -5 (*E-3m* and *E-3j*). Scores for the S-site ranged from -1.95 to -5.41 with all but one compound (*E-3r*) reporting poor docking scores. While *E-3m*, *E-3j*, and *E-3r* showed some favorable interactions with either the A-site or S-site, all analogs reported much higher docking scores for the C-site, suggesting that these analogs are more likely to inhibit hRR by binding to the C-site.

By using the now well-defined pan-assay interference compounds¹¹ (PAINS) filter as a gateway parameter, we monitored the presence or absence of potentially problematic functional groups in our analog design. Despite being a potential PAINS candidate, the validity of parent *E-3a* as a lead compound was greatly strengthened by the crystal structure data that showed binding of *E-3a* to the C-site of RR.¹⁰ A subset of analogs, *E-3a*, *E-3c*, *E-3f*, *E-3s*, *E-3t* and *E-3u*, displayed favorable docking poses as shown in Figure 2 upon docking to the C-site of hRR. They were primary synthetic targets in our design leading to twenty additional analogs.

Synthesis of Naphthyl Salicylacylhydrazone analogs

We constructed a library of salicyl-derived acyl hydrazones (Scheme 1A) based upon *in silico* screening results. The synthetic method yielded a library of analogs through a five-step sequence from commercially available acids in high overall yields. Specifically,

salicylic acid derivatives (**1**) were converted to their corresponding methyl esters and subsequently transformed into corresponding acylhydrazides (**2**) under the treatment with hydrazine hydrate in methanol. Naphthyl ring containing acids (**4**), were reduced to their primary alcohol using lithium aluminum hydride in diethyl ether and the resulting alcohols were re-oxidized with pyridinium chlorochromate (PCC) in dichloromethane at room temperature to yield several aldehydes as represented by **5**. The resulting aldehydes were condensed with acyl hydrazides (**2**) with catalytic amount of glacial acetic acid under reflux over 3–4 h. This step resulted in the generation of *E*-**3a** as the major product whose identity was verified using ¹H, ¹³C-NMR and high resolution mass spectrometry (See SI). Detailed step-wise description of the synthesis is provided in the SI. Our synthetic pathway, by virtue of employing higher temperatures during the final condensation step involving **2** and **5**, uniformly afforded the thermally more stable *E*-isomer in all cases. Though Scheme 1 outlines the theoretical possibility of a photoisomerization equilibrium that may exist between the two configurational isomers of **3A** (*E* and *Z* isomers), in practice we observe only *E*-isomers to be formed. We observe a possible influence of severe allylic (A^{1,3}) strain in the *Z*-isomer (which forces 6 atoms including the hydrazone nitrogens and the naphthyl carbons and the hydroxyl group to be in one plane) thermodynamically favoring the *E*-isomer to be the sole product in our synthesis.

Recently, acylhydrazones with unique λ_{\max} per geometrical isomers were characterized as new class of highly tunable photoswitching compounds.¹² Through UV emission spectroscopy, we measured a λ_{\max} of 320 nm attributable to the acyl hydrazone functionality in the *trans* configuration (Scheme 1B). It is the *E*-isomer that crystallized with hRRM1 in the recent report we published and used as a template herein.¹⁰ The *E* and *Z* isomers are expected to show distinct biological efficacy, and therefore throughout this work we have characterized the major *E*-isomer as a single component, in each analog case, and depict them with the *E*-notation.

Synthesis of most of the analogs followed the sequence as shown in Scheme 1, with the exception of sulfonyl hydrazones (*E*-**3s**, *E*-**3o**, *E*-**3r** and *E*-**3q**) that were obtained by a slightly modified procedure (See SI). A few diimino hydrazones were obtained through a bi-directional imine condensation with aldehydes that deviated slightly from general procedures described for reactions in Scheme 1 (See SI). Nevertheless, all analogs were neatly obtained as purified products in moderate to high yields (> 60–90 %) and the reactions were easy to perform on multi-gram quantities. Overall, twenty-five analogs were prepared for biological evaluations and their inhibitory properties are listed in Table 1.

Enzymatic inhibition assays reveal favourable substitutions for increasing potency

The parent inhibitor and its analogs (*E*-**3a-z**) were subjected to enzymatic inhibition assays and ranked according to their IC₅₀s. All of the analogs that were evaluated reported IC₅₀s in the micromolar range, with subtle variations in structure leading to observable differences in potencies. Of the top ranked hydrazones based on their IC₅₀ values, five compounds (*E*-**3f**, *E*-**3c**, *E*-**3t**, *E*-**3s** and *E*-**3z** as listed in Table 1, **group A** (above) showed ~ 2–4-fold improvement from the initial IC₅₀ of 19 μ M for our lead compound *E*-**3a**. Pyridyl ring-containing *E*-**3f** (IC₅₀ ~ 5.3 μ M), *E*-**3c** consisting of a 6-hydroxy naphthyl ring (IC₅₀ ~ 7.3

μM), *p*-methyl substituted aryl sulfonamide containing *E-3s* ($\text{IC}_{50} \sim 6.8 \mu\text{M}$), and *p*-amino-*m*-chloro substituted *E-3t* ($\text{IC}_{50} \sim 6.1 \mu\text{M}$) analogs showed the greatest improvement from *E-3a* with IC_{50} s below $10 \mu\text{M}$, as listed in Table 1, **group A** (above). Interestingly, *E-3z* ($\text{IC}_{50} \sim 10.2 \mu\text{M}$) consisting of an C3-derived indole ring system in place of the naphthyl ring, retained its potency despite the change in the heterocyclic ring system. The single point structural change occurring on either of the two flanking aromatic rings on either side of the hydrazone core impacted IC_{50} s of analogs. The importance of these substitutions were predicted earlier through the *in silico* screening, where these five analogs were identified as top choices. For example, the C-site Ser 606 and Thr 607 display shorter hydrogen bonding interactions with the acyl group of *E-3a* and at least one more stabilizing interaction comes from an additional hydrogen bond due to the presence of polar hydroxyl or amino groups on the aromatic ring system on these inhibitors as depicted in Figure 2B–F (above). For *E-3s*, a sulfonyl hydrazone, both O atoms connected to S engage in hydrogen bonding interactions favoring the binding of these analogs at the C-site of hRR. For naphthalene substitutions containing a C6-hydroxy group (*E-3c*), the main chain of Pro 294 engages in a stronger hydrogen bonding interaction as depicted in Figure 2B. *E-3w*, *E-3u*, *E-3v*, *E-3y* and *E-3n* showed modest improvements from the lead compound as ranked in Table 1, **group B** (above). Analog *E-3y*, *E-3n* and *E-3z* (from **group A**) contain an indole ring system replacing the naphthalene core of lead compounds. This change resulted in preserving, or even improving (*E-3z*), the efficacy afforded by the naphthalene ring system. These analogs are a favorable choice for further refinement because it is easier to derivatize indole ring-containing compounds than the naphthalene ring core of these inhibitors. Besides the six most potent inhibitors shown in Figure 2, docking poses revealing contacts between the remaining nine inhibitors and the hRR C-site are presented in Figures S1–S9 (see SI). Together, these data provide a roadmap for designing second generation non-nucleosidic RR inhibitors.

Seven of the 12 analogs reporting IC_{50} s below $24 \mu\text{M}$ have a polar group positioned *ortho* to the hydrazone chain on the benzene ring, while another three feature a polar group in the *meta* position, as shown in Table 1, **group C** (above). The majority of para-substituted analogs, however, showed a marked decrease in activity. This suggests that the *ortho*-polar substitution is critical to enhancing hRR inhibition. While *E-3s* showed improvement in potency towards hRR, all other sulfonyl hydrazones became less potent than the lead compound, suggesting that this functional change is sensitive to the pendant hydrophobic groups present on either side of the hydrazone core. Moving the hydroxyl group of the naphthalene ring from carbon 2 to carbon 6 improved the potency toward RR by approximately 3-fold, supporting the prediction made by structure guided design that this substitution would hydrogen bond more favorably within the catalytic C-site of hRR. Additionally, substituting the naphthalene ring with an indole derivative showed no loss in potency, suggesting that the two ring systems are equivalent toward hRR inhibition. Of the five halogenated analogs tested, four showed an increased potency toward RR.

By these observations, a broad pharmacophore for these analogs can be developed incorporating *ortho* substitution of polar groups on both the benzene and naphthalene ring systems. Substitutions which interact with Ser 606, Thr 607, and Pro 294 are considered

favorable for improving inhibitory potency. Additionally, substitution of the naphthalene ring for an indole ring can be used to access additional substitutions not readily available from a naphthalene ring system while fragment growth can be directed from the para position of the benzene ring system. Together, these observations provide a guide for future lead optimization of this class of hRR inhibitors.

NSAHs do not inhibit hRR through sequestering catalytically essential Fe

There are multiple reports of small molecule agents that inhibit RR through the scavenging of free radicals that are required for the reduction of nucleoside diphosphates. Nitric oxide¹³ and hydroxyurea¹⁴ (that quench the tyrosyl free radicals), and iron chelating small molecules¹⁵ such as desferrioxamine (that irreversibly chelate to Fe (II) that is essential for housing the free radical) are a few examples. Because the basic scaffold of these inhibitors possessed a possible chelating functional group that involves the 2-OH substituent on the naphthyl ring along with the hydrazone-imino N, we wondered if a metal chelating mechanism may contribute to its inhibitory mode of action against hRR. Therefore, to test this hypothesis, the propensity of *E-3a* to bind to Fe³⁺ and Fe²⁺ was studied by UV spectroscopy. In 10 mM ammonium acetate buffer (pH 7.0) under anaerobic conditions, a 100 μ M solution of *E-3a* was treated with FeCl₂·6H₂O or FeCl₃·6H₂O at varying concentrations of metal ranging from 100 μ M to 5 mM. The stoichiometry of *E-3a*: MX⁺ tested were 1:1, 1:2, 1:3, 1:4, 1:5, 1:6, 1:7, 1:8, 1:9, 1:10, 1:20, and 1:50. A scanning UV emission spectrum was recorded between 200–800 nm at each concentration. Noticeable changes occurred when *E-3a* was subjected to a titration with FeCl₂·6H₂O at concentrations of metal ranging from 400 μ M to 1 mM. At concentrations above 1 mM, the UV detector was saturated and the UV profile of the ligand-metal complex could not be readily obtained. Once the *E-3a*:Fe²⁺ ion stoichiometry reached, or exceeded a 1:4 ratio, the UV emission spectrum revealed mild changes reflecting that the ligand was in a bound state with Fe²⁺. Similarly, a titration experiment was carried against Fe³⁺ salt at concentrations of metal ranging from 100 μ M to 5 mM at stoichiometry of 1:1, 1:2, 1:3, 1:4, 1:5, 1:6, 1:7, 1:8, 1:9, 1:10, 1:20, and 1:50. There were no noticeable changes in UV emission spectra at any of these stoichiometry for Fe³⁺ ions, indicating that *E-3a* does not chelate Fe³⁺ ions. Taken together, these results support the conclusion that while *E-3a* does not inhibit hRR through metal chelation or sequestration of Fe³⁺, *E-3a* may participate in a chelation mechanism in the presence of excess Fe²⁺. Results supporting these observations are presented in Figures S10–S11 (See SI). We reviewed the potential of these inhibitors to chelate Mg²⁺ ions as well, because these ions are present in the *in vitro* enzyme assay buffer for hRR inhibition. Per spectra shown in Figure S12 (See SI) we conclusively show that these compounds do not bind and sequester Mg²⁺ ions.

NSAH analogs inhibit hRR competitively and reversibly

In a recently published study¹⁰, using multiple lines of investigations involving steady-state inhibition kinetics, a jump-dilution assay and an *in vitro* hRRM1 fluorescence-quenching assay, we have gathered evidence that the lead inhibitor, *E-3a* inhibited hRR in a reversible, competitive manner with an IC₅₀ of 32 ± 10.2 μ M and a dissociation constant (K_D) of 37 ± 4.7 μ M.¹⁰ We initially suspected that due to the presence of an unsubstituted electrophilic azomethine carbon (C=N) on the parent pharmacophore, this inhibitor could irreversibly

inactivate the enzyme, by forming covalent bonds with nucleophilic residues at the C-site. Though the 2.7 Å X-ray structure did not support this model, further detailed kinetic analyses were undertaken for further confirmation. In order to verify the potential of *E-3a* to reversibly inhibit hRRM1 at its C-site, a preincubation-dilution experiment was performed as outlined in the parallel study.¹⁰ Results from that analysis point to reversible inhibition of the enzyme whose activity could be resuscitated upon diluting away the inhibitor. Further analyses using steady state-kinetics revealed a model consistent with competitive inhibition, and correspondingly the K_i value of *E-3a* was evaluated to be 5.0 μM .

To verify that new analogs of the parent inhibitor (*E-3a*) follow the same mode of inhibition of hRRM1 in this study, we subjected the most potent analogs, *E-3a* (as positive control), *E-3c*, *E-3t*, and *E-3w* analysis by steady-state inhibition kinetics. Double-reciprocal plots were prepared for wild type hRRM1 at varying substrate concentrations and hRRM1 in the presence of these each of the four inhibitors, independently at concentrations of 100 μM , 50 μM , 25 μM , 10 μM , and 5 μM respectively. As shown in Figure 3A (below), the double-reciprocal plot of *E-3a* inhibition against hRRM1 indicates that all data sets converge upon a common y-intercept near the origin, indicative of the fact that K_m of the inhibitor is dependent upon inhibitor concentration [I] while V_{max} is independent of [I], consistent with a competitive mechanism of inhibition. As shown in Figure 3B, C and D (below), a similar trend was observed for *E-3c*, *E-3t*, and *E-3w* respectively, indicating that like *E-3a*, the K_m of these analogs is dependent upon [I] while V_{max} is independent of [I]. Overall, these observations suggest that *E-3c*, *E-3t*, and *E-3w* are competitive inhibitors in the same manner as the parent inhibitor *E-3a*.

For the kinetic analysis outlined above, the sigmoidal dose response curves for *E-3a* (as positive control), *E-3c*, *E-3t*, and *E-3w* are provided in Figure S13 (see SI). It is noteworthy that our recent discovery of the crystal structure data of *E-3a* in complex with hRRM1 shows the inhibitor bound at the C-site of the enzyme, corroborating our kinetic model of inhibition.¹⁰ Because ADP-reductase activity is one of the lowest among all NDPs (<50 U/mg) and thereby usually has a low dynamic range, we further tested these inhibitors with a ³H-CDP assay method. Specific activity of wild-type R1 (ranging between 450–481 nmol $\text{min}^{-1} \text{mg}^{-1}$) as well as IC_{50} values calculated for inhibitors *E-3a*, *E-3c*, *E-3t*, and *E-3w* correlate with those values obtained through the ¹⁴C-ADP substrate method, negating the need to repeat the remaining ¹⁴C-ADP IC_{50} measurements. Data supporting this correlation is provided in the supporting information (Table S4).

As the acylhydrazone core of this library of inhibitors is structurally similar to the thiosemicarbazone functionality present in the known R2 inhibitor and metal chelator triapine, it was necessary to determine if the overall mode of inhibition for these inhibitors in this series involve targeting of hRRM2. In order to probe this aspect, enzymatic inhibition assays were used to determine the enzymatic IC_{50} values for triapine (as a control) and compare its efficacy to that of *E-3a* against hRRM2. The specific activity of wild type hRRM2 in the presence of triapine (at varying concentrations of 100, 50, 5, 0.2, 0.50, and 0.10 μM) and *E-3a* (at varying concentrations of 5,000, 400, 100, 50, 5, 0.2, 0.50, and 0.10 μM) were normalized, then plotted against the logarithm [I]. The data were fitted to a sigmoidal dose-response curve to determine the IC_{50} values of triapine and *E-3a*, as 0.185

μM and $123 \mu\text{M}$ respectively (Figure 4, below). As the IC_{50} for *E-3a* is approximately 1,000-fold that observed for triapine, and approximately 6 times greater than the IC_{50} value for *E-3a* against hRRM1, it is unlikely that hRRM2 is a significant cellular target of *E-3a*.

siRNA knockdown approach further points to RR targeting mode of action *in vivo*

Previous work from our group demonstrated changes in dNTP pools and cell cycle progression after treatment with (NSAH) *E-3a*.¹⁰ Although generally measurements of perturbations to cellular dNTP pool, in tandem with cell cycle arrest, has been used to identify cellular RR activity¹⁶ (Bianchi 1986; Lagergren 1987) additional confirmation can be derived using siRNA by Reid *et al.*¹⁷ or using inducible shRNA by Wisitpitthaya *et al.*^{4d} to repress RR. The siRNA approach measuring the level of sensitization that a drug renders to RR under knocked-down conditions has been previously utilized to verify the cellular inhibition of RRM1 by gemcitabine and RRM2 by hydroxyurea¹⁷ and to delineate the role of RR oligomerization in the activity of clinically relevant inhibitors^{4d}. To identify optimal levels of RRM1 repression for NSAH sensitivity testing, we transfected a range of validated siRNAs (specific for RRM1, 3 RefSeqs, ThermoFisher Silencer® Select, s12358; and control scrambled siRNAs), and assessed cell growth over a 48-hour period (SI Figure S14). As expected, significant inhibition of RRM1 resulted in growth inhibition, with an IC_{50} of approximately 3 pmoles/well, while the control scrambled siRNAs showed less than 50% growth inhibition even at 20 pmole/well, the highest amount tested. This guided the selection of the range of siRNA amounts (1–5 pmoles siRNA/well) used in the inhibitor treatment studies. For drug sensitivity study, cells were transfected with RRM1 or control scrambled siRNAs, followed 48 hours later by administration of *E-3a*. Relative growth inhibition was assessed after incubation for an additional 5 days. As shown in Figure 5, the relative NSAH-inhibitor induced growth inhibition in cells with siRNA-mediated knockdown of RRM1 was greater than that in cells with endogenous levels of RRM1.

The relative differences in DNA content in respective treatments were measured and are shown in SI Figure S15. The relative growth inhibition in cells treated with 4 pmol siRNA ($\text{IC}_{50} = 0.347 \mu\text{M}$) was greater than that observed with lesser amounts of RRM1 siRNA (2 pmol $\text{IC}_{50} = 1.43 \mu\text{M}$) or any quantity of Control siRNA (4 pmol $\text{IC}_{50} = 1.94 \mu\text{M}$), or no siRNA ($\text{IC}_{50} = 1.49 \mu\text{M}$), indicating that suppression of RRM1 caused sensitization to NSAH, further supporting its RRM1 specific mode of action.

Cytotoxicity studies of NSAH inhibitor analogs

Similar to a recently published study from our group¹⁰, the entire suite of inhibitors (*E-3a-z*) were concurrently evaluated for their cellular effects against both human colon cancer (HCT116) and human breast cancer (MDA-MB-231) cell lines. Continuous 72-hour exposure of *E-3a* and gemcitabine (as a control) demonstrated growth inhibition in both human cancer cell lines. IC_{50} s for gemcitabine ranged between 30 and 100 nM. *E-3a* displays cytotoxicity against HCT116 cells with an IC_{50} of 225 nM while displaying cytotoxicity against MDA-MB-231 cells with an IC_{50} of 300 nM.¹⁰ Analogs *E-3o* and *E-3v* display cytotoxicity against HCT116 cells with IC_{50} 's of 10 and 1 μM respectively. The remaining analogs did not exhibit significant cytotoxicity. Their net cytotoxicity effect is summarized in Table S2 (see SI). As illustrated in Table S2, not all inhibitors in this series

exhibited significant levels of cytotoxicity. This observation correlated partly with the fact that not all inhibitors in this series were sufficiently soluble in cell culture media, with compound precipitation resulting in insignificant cytotoxicity for many analogs. Therefore, detailed cellular toxicity results could be obtained only for *E-3a*, *E-3o* and *E-3v*. In many cases, a cancer cell cytotoxicity with cellular IC₅₀ of >10 μM may primarily be an effect due to high insolubility of the inhibitor, underscoring the importance of solubility (in biologically relevant environments) for future improvements in potency.

Discussion and Conclusion

Although acylhydrazones display a wide range of biological activities, including inhibition of metazoan proteases¹⁸, anti-*Leishmania* properties¹⁹, herbicidal effects²⁰, and inhibition of proliferating cellular nuclear antigen (PCNA)²¹, we were the first to discover that naphthyl Salicyl acylhydrazones (especially the lead inhibitor *E-3a*) inhibit hRR through binding at the C-site of RRM1.¹⁰ In this study, we establish a hydrazone pharmacophore inactivating hRR in a reversible, competitive mode through binding at the C-site of the enzyme. As such, we rationalized that structure-based design could be used in tandem with structure-activity relationship studies to further develop our understanding of how acylhydrazones could be used to target hRR for cancer treatment.

Most of the clinically used RR inhibitors are nucleoside analogs such as gemcitabine, which is currently used to treat pancreatic cancer. Gemcitabine has been shown to inhibit RR in a synergistic manner, with irreversible hRR inhibition and depleted nucleotide pools allowing for gemcitabine triphosphate to become incorporated into growing DNA strands by DNA polymerase, causing delayed chain termination and triggering apoptosis. This mechanism does not distinguish between normal and cancerous cells, and therefore gemcitabine is associated with serious side effects due to toxicity towards normal cells resulting from DNA chain termination, irreversible inhibition of hRR, and inhibition of other enzymes such as topoisomerase-1, thymidylate synthase, deoxycytidine deaminase, CTP-synthase, which recognize phosphate moieties.^{6,7} This combination of indiscriminate cross-reactivity, irreversible inhibition, and DNA chain termination produces undesirable cytotoxicity in normal cells and thereby results in a relatively low therapeutic index when use in the treatment of patients. We therefore hypothesize that identification and characterization of specific, reversible, non-nucleoside RR inhibitors could prove advantageous by reducing the cytotoxicity towards normal cells caused by nucleoside analogs.

While previous RR inhibitors display a diverse range of mechanisms of inhibition, there have been few efforts to identify reversible, non-nucleosidic small molecules that inhibit the hRRM1 subunit. In Ahmad *et.al.* 2015, we reported a rapid throughput screening method integrating *in silico* docking, cell-based assays, and biochemical experiments which identified ten novel classes of non-nucleosidic RR inhibitors.⁸ This study marked the first compounds identified to inhibit RR by binding to a protein-protein interface (M-site) and inducing formation of catalytically inactive hexamers. Recently, we reported the identification of the first non-nucleoside identified to bind to the C-site of hRR (PDB ID: 5TUS).¹⁰ This lead inhibitor *E-3a*, an acylhydrazone, was determined to inhibit RR in a

reversible, competitive manner and exhibit potent cytotoxicity towards multiple cancer cell lines.

Using the crystal structure of *E-3a* in complex with hRRM1 (PDB ID: 5TUS)¹⁰ as a template, a focused library of analogs was designed using *in silico* modeling. *In silico* docking with the Schrödinger software suite was used to evaluate 100 analogs and the top 25 were selected based upon the predicted docking poses. A modular, *E*-isomer selective synthetic pathway was implemented which afforded hydrazones on a multi-gram scale in five steps with isolated yields ranging between 65 and 85% typically, with a few exceptions. *In vitro* RR inhibition assays identified five analogs with 2–4 fold improvement in IC₅₀ from the lead compound, *E-3a*. All five analogs were predicted to be more potent toward RR during the *in silico* modeling, as all of these analogs showed shorter hydrogen bonding interactions with residues Ser 606, Thr 607, and Ser 217, which are known to hydrogen bond with natural nucleoside substrates. It was also determined that the *ortho* substitution of a polar group on either ring system was critical for RR inhibition, while substitution of the naphthalene ring system for an indole ring resulted in no loss in activity, providing potential access to a broader range of chemical derivatives. Upon evaluating *in vitro* inhibitory potencies against hRR, broadly a subset of 15 inhibitors were identified within a narrow range of IC₅₀s.

Due to the presence of a hydrazone functionality on the parent inhibitor structure, we were concerned that this group had the propensity to be attacked by an active site nucleophile (e.g. Cys 429) present in hRR, thereby irreversibly inactivating the enzyme. The data presented in Figure 3 provided us with a mechanistic model of inhibition for these inhibitors. The participation of the hydrazone azomethine nitrogen and the C=N bond through a covalent mode can be ruled out, and reversible inhibitory modes can be invoked. Metal chelation assays determined that *E-3a* does not chelate Fe³⁺ ions, however Fe²⁺ complexation was observed in the presence of excess Fe²⁺ (4-fold excess and higher). While the X-ray crystal data obtained in a previous study strongly suggests that the biological activity of *E-3a*-like compounds can be attributed to inhibition of RR, a separate metal chelation mechanism cannot be completely ruled out, especially when relatively high Fe²⁺ ion concentrations may be present in cells (typically > 1 mM). Importantly, analogs *E-3c*, *E-3t*, and *E-3w* were all determined to inhibit hRR through similar competitive, reversible mechanisms as the lead compound (*E-3a*), suggesting that novel analogs possessing this pharmacophore follow the same mechanism of inhibition as the lead compound.

The relatively large difference between the mid-micromolar enzymatic IC₅₀ (*in vitro*) and nanomolar cellular IC₅₀ (against cancer cells *in vivo*) suggested that *E-3a* may interact with multiple targets. This raised a concern regarding whether hRR is indeed a cellular target. In a recently published study, we evaluated the perturbation of cellular dNTP levels specifically in the presence of *E-3a*, and compared them to levels in cells treated with hydroxyurea, at their respective IC₅₀s.¹⁰ The addition of *E-3a* was shown to induce a pattern of dNTP depletion with greatest depletion of dATP and dGTP, with little or no effect on dCTP or dTTP levels. This was followed by an arrest of cells in early S-phase. These observations are similar to patterns observed with gemcitabine and hydroxyurea and comprise a signature for a cellular hRR inhibitor.²² Using mobilized peripheral blood progenitor cells (a common

target for dose limiting toxicity during gemcitabine therapy), *E-3a* was shown to have a superior therapeutic index compared to gemcitabine.¹⁰ These observations point to promising selective cytotoxicity attributable to hRR inhibition by *E-3a*. Analogs *E-3o* and *E-3v*, showing similar cytotoxicity profile as *E-3a*, may also be expected to target hRR *in vivo*. However, we are cognizant of the possibility that inhibitors like *E-3a* and its analogs may possibly engage multiple cellular targets that are yet to be identified.

It is generally agreed that RR is a challenging therapeutic target for cancer, as inhibitors are unlikely to distinguish between malignant and normal cells. We recently demonstrated that in blood progenitor cells, inhibitor *E-3a* showed a superior therapeutic index in comparison with gemcitabine, suggesting a possible discrimination between transformed and untransformed cells.¹⁰ We wish to further exploit this new class of inhibitors for the possible treatment of cancer, especially against gemcitabine-resistant forms. In the long term, identification of non-nucleoside, reversible RR inhibitors may provide an avenue towards developing safer alternatives to irreversible nucleoside analogs as chemotherapeutic agents. Furthermore, considering the fact that RR broadly impacts multiple pathologies, these reversible agents may impact drug discovery for treatment of a wider range of proliferative diseases.

Experimental Section

***In Silico* docking with Schrödinger suite for predicting C-site binding affinity**

In silico docking of each hydrazone analog was performed using the Glide docking module of the Schrödinger 9.3 modeling software suite as previously described in Ahmed and Huff *et al.*⁸ The docking site was defined as a box of 5 Å centered on the original hydrazone ligand in the hR1 complex (PDB ID: 5TUS). Ligands were then docked to the catalytic site using Glide XP. The generated docking poses were evaluated for interactions with residues that commonly bind to natural substrates, such as Ser 202, Ser 606, Gly 246, and Arg 293. Ligands that showed favorable interactions with these residues were selected for synthesis. Generally, most inhibitors screened here showed very minimal perturbation or binding interaction with C-site residues involved in catalysis, such as Glu 431, Cys 429, Cys 444, Cys 218 and Asn 427. Therefore, these sites were omitted from depiction in the docked poses with inhibitors. Specific docking poses for inhibitors that showed lower than 5–10 μM potency (IC₅₀) are depicted in Figures S1-S9 (see SI).

***In Silico* docking with Schrödinger suite for predicting site selectivity**

Proteins and ligands were prepared as described below. Docking of the S-site and A-site was performed using the previously determined ATP-TTP-hRRM1 crystal structure (PDB ID: 3HNE). The S-site docking grid was defined as a 5 Å cube (125 Å³) centered on the TTP ligand. The A-site docking grid was defined as a 5 Å cube (125 Å³) centered on the ATP ligand. Docking scores for each inhibitor docked to each of the three sites are reported in Table S3.

Human ribonucleotide reductase protein expression and purification

The hRRM1 protein was expressed in *E. coli* BL21-codon plus (DE3)-RIL cells and purified using peptide affinity chromatography as previously described in Fairman *et. al.*^{5c} The hRRM2 protein was also expressed in *E. coli* BL21-codon plus (DE3) cells and purified to homogeneity using Ni-NTA affinity chromatography as described in Fairman *et. al.*^{5c} Iron was loaded into the hRRM2 subunit as described in Ahmed and Huff *et. al.*⁸ Concentration of the homogeneous protein was quantified using UV spectroscopy.

Ribonucleotide reductase *in vitro* inhibition assay

[¹⁴C]-ADP reduction assay—The *in vitro* specific activity of human ribonucleotide reductase was determined by ¹⁴C-ADP reduction assays using a reaction mixture of 0.3 μM hRRM1 and 2.1 μM hRRM2 in an activity assay buffer containing 50 mM HEPES (pH 7.6), 15 mM MgCl₂, 1 mM EDTA, 100 mM KCl, 5 mM DTT, 3 mM ATP, 100 μM dGTP and 1 mM ¹⁴C-ADP (~3000 cpm/nmol). The reaction mixture was pre-incubated for 3 min at 37 °C, and 30 μL aliquots were sampled at fixed time intervals after initiation of the reaction. Reactions were quenched by immersion in a boiling water bath. The aliquots were then cooled and treated with alkaline phosphatase for 2 hours. The product ¹⁴C-dADP that formed during the reaction was separated from substrate ¹⁴C-ADP using boronate affinity chromatography. Amount of [¹⁴C]-dADP formed from the reaction was quantified by liquid scintillation counting using a Beckman LS6500 liquid scintillation counter. The assays were repeated in triplicate and the averaged specific activities were used for IC₅₀ calculations.

[³H]-CDP reduction assay—Assays to determine the IC₅₀ values for compounds **3a**, **3c**, **3t**, and **3w** in the presence of ³H-CDP substrate were performed with a reaction mixture consisting of 0.3 μM hRRM1 and 2.1 μM hRRM2 in an activity assay buffer of 50 mM HEPES (pH 7.6), 15 mM MgCl₂, 1 mM EDTA, 100 mM KCl, 5 mM DTT, 3 mM ATP, 100 μM dGTP and 1 mM ³H-CDP (~2000 cpm/nmol). After processing of the reaction similar to the procedure described above, the amount of [³H]-dCDP formed from the reaction was quantified by liquid scintillation counting using a Beckman LS6500 liquid scintillation counter. The assays were repeated in triplicate and the raw specific activities are reported below in Table S2 (see SI).

[¹⁴C]-ADP assays to determine inhibition of the hRRM2 subunit—These assays were performed as with reaction mixture of 2.1 μM hRRM1 and 0.3 μM hRRM2 in an activity assay buffer of 50 mM HEPES pH 7.6, 15 mM MgCl₂, 1 mM EDTA, 100 mM KCl, 5 mM DTT, 3 mM ATP, 100 μM dGTP and 1 mM ¹⁴C-ADP (~3000 cpm/nmol). The specific activity was determined for wild type hRRM2, and hRRM2 in the presence of triapine (at 100 μM, 50 μM, 5 μM, 0.2 μM, 0.05 μM, and 0.01 μM concentrations) or **3A** (at 5,000 μM, 400 μM, 100 μM, 50 μM, 0.2 μM, 0.05 μM, and 0.01 μM concentrations) respectively. After processing of the reaction similar to the procedure described above, the amount of [¹⁴C]-dADP formed from the reaction was quantified by liquid scintillation counting using a Beckman LS6500 liquid scintillation counter. All assays were repeated in triplicate and reported values are averaged.

Assays in the presence of E-3a inhibitor analogs—All compounds were dissolved in 100% DMSO and diluted to the appropriate concentration so that the total DMSO volume in the reaction mixture did not exceed 0.2%. At this concentration of DMSO, the loss of RR activity is less than 1%. The IC₅₀ was defined as the concentration of any compound that reduced the specific activity of hRRM1 to 50% of the control activity. A two-point assay for IC₅₀ determination was adopted from the procedure described in Ahmed *et al.*⁸ for most inhibitors tested. Based on this method, concentrations of 5 and 100 μM of the inhibitor were used for estimating the IC₅₀. All assays were repeated in triplicate and reported values are averaged.

Assays to Determine Mode of RR Inhibition—The IC₅₀s of **3a**, **3c**, **3t**, and **3w** were determined as previously described using inhibitor concentrations of 5 μM, 10 μM, 25 μM, 50 μM, and 100 μM respectively. The IC₅₀s for these three analogs were determined for substrate concentrations of 0.5 mM, 1.0 mM, and 1.5 mM of ¹⁴C-ADP to determine if changes in substrate concentration influenced the observed IC₅₀. All assays were repeated in triplicate and averages are reported.

Compound Characterization—Supporting information provides details on solvent purification and general methods followed for synthesis and purification of each analog reported herein. Each analog reported as a novel compound in this study was purified using column chromatography or crystallization methods before characterization of their identity and purity. All reported yields for final products were for compounds that are >95% pure. The purity was evaluated to be > 95% using NMR and HPLC methods whose copies are provided in the supporting information.

2-hydroxy-*N*'-((2-hydroxynaphthalen-1-yl)methylene)benzohydrazide (3a)—

According to general procedure D (see SI), a 1:1 molar ratio of salicylic hydrazide (760 mg, 5 mmol) and 2-hydroxy-1-naphthaldehyde (861 mg, 5 mmol) were dissolved in 30 mL of MeOH and heated to reflux. Several drops of glacial acetic acid were added to catalyze the reaction and the flask was heated at reflux for 3–4 h. The reaction mixture was filtered to collect the crude product as a yellow precipitate, and the compound **3a** was purified by silica gel column chromatography (1.38 g, 4.51 mmol; 90% yield). IR: 3500-3200 (broad, OH), 3046 (aromatic C-H), 2114 (C=N), 1639 (C=O), 1550 (C=C), 1236 (C-O), 744 (*o* substitution). ¹H-NMR: (CD₃CN, 500 MHz) 12.90 (s, 1H), 11.85 (s, 1H), 10.94 (s, 1H), 9.52 (s, 1H), 8.21 (d, *J* = 8.6 Hz, 1H), 8.02 (d, *J* = 8.7, 1H), 7.97 (d, *J* = 8.7 Hz, 1H), 7.92 (m, 1H), 7.72 (t, *J* = 7.8 Hz, 1H), 7.61 (t, *J* = 7.7 Hz, 1H), 7.53 (t, *J* = 7.6 Hz, 1H), 7.33 (m, 1H), 7.12 (m, *J* = 8.2 Hz, 2H). ¹³C-NMR: (CD₃CN, 125 MHz) 164.9, 159.6, 159.0, 148.5, 135.4, 133.8, 132.6, 129.8, 129.6, 128.4, 127.5, 124.3, 120.6, 119.7, 119.6, 118.5, 116.6, 109.5. HRMS (ESI, [M+Na]⁺) *m/z* calcd. for C₁₈H₁₄N₂O₃Na 329.0902, found: 329.0895.

2-hydroxy-*N*'-((6-hydroxynaphthalen-2-yl)methylene)benzohydrazide (3c)—

Prepared according to general procedures described in the SI. Yield 1.07 g, 3.50 mmol; 72% yield. Yellow solid, mp 230 °C. IR: 3415 (secondary NH), 3300-3200 (broad, OH), 2250 (C=N), 1628 (C=O), 1543 (C=C), 1204 (C-O). ¹H-NMR: ((CD₃)₂SO, 500 MHz) δ 12.50 (s, 1H), 10.21 (s, 1H), 10.04 (s, 1H), 8.49 (s, 1H), 7.98 (d, *J* = 8.7 Hz, 1H), 7.86 (d, *J* = 8.4 Hz,

1H), 7.84 (d, $J = 8.4$ Hz, 1H), 7.78 (t, $J = 8.4$ Hz, 1H), 7.37 (ddd, $J = 8.5, 7.2, 1.7$ Hz, 1H), 7.21-7.12 (m, 3H), 6.92-6.80 (m, 2H). $^{13}\text{C-NMR}$: (CD_3CN , 125 MHz) 168.4, 167.0, 160.1, 158.2, 137.6, 134.9, 132.2, 131.5, 127.4, 127.0, 126.4, 125.6, 124.1, 120.1, 119.7, 118.6, 114.8, 109.9. HRMS (ESI, $[\text{M}+\text{Na}]^+$) m/z calcd. for $\text{C}_{18}\text{H}_{14}\text{N}_2\text{O}_3\text{Na}$ 329.0902, found: 329.0915.

2-amino-*N'*-((2-hydroxynaphthalen-1-yl)methylene)benzohydrazide (3e)—

Prepared according to general procedures described in the SI. Yield 1.16 g, 3.82 mmol; 76%. Yellow solid, mp 229 °C. IR: 3451 (primary NH), 3300-3250 (broad, OH), 2117 (C=N), 1618 (C=O), 1577 (C=C), 1240 (C-N), 1182 (C-O). $^1\text{H-NMR}$: ($(\text{CD}_3)_2\text{SO}$, 500 MHz) δ 12.89 (s, 1H), 10.00 (s, 1H), 9.02 (s, 1H), 8.65 (d, $J = 8.7$ Hz, 1H), 8.04 (d, $J = 9.0$ Hz, 1H), 7.92 (d, $J = 8.0$ Hz, 1H), 7.62 (t, $J = 7.8$ Hz, 1H), 7.52 (t, $J = 7.4$ Hz, 1H), 7.44 (t, $J = 7.4$ Hz, 1H), 7.29 (d, $J = 9.0$ Hz, 1H), 7.12 (d, $J = 8.2$ Hz, 1H), 6.92-6.89 (m, 2H), 5.34-5.27 (m, 2H). $^{13}\text{C-NMR}$: ($(\text{CD}_3)_2\text{SO}$, 125 MHz) 168.1, 165.2, 148.4, 143.3, 134.9, 133.5, 132.2, 129.3, 128.2, 128.1, 127.6, 123.9, 120.1, 119.4, 119.2, 118.7, 113.7, 109.0. HRMS (ESI, $[\text{M}+\text{Na}]^+$) m/z calcd. for $\text{C}_{18}\text{H}_{15}\text{N}_3\text{O}_2\text{Na}$ 328.1056, found: 328.1061.

***N'*-((2-hydroxynaphthalen-1-yl)methylene)nicotinohydrazide (3f)**—Prepared

according to general procedures described in the SI. Yield 1.19 g, 4.08 mmol; 82%. Yellow solid; mp 231 °C. IR: 3415 (secondary NH), 3300-3200 (broad, OH), 2107 (C=N), 1619 (C=O), 1577 (C=C), 1140 (C-O). $^1\text{H-NMR}$: ($(\text{CD}_3)_2\text{SO}$, 500 MHz) δ 12.60 (s, 1H), 12.37 (s, 1H), 9.47 (s, 1H), 9.15 (s, 1H), 8.81 (d, $J = 4.7$ Hz, 1H), 8.33 (d, $J = 8.0$ Hz, 1H), 8.30 (d, $J = 8.0$ Hz, 1H), 7.96 (d, $J = 8.5$ Hz, 1H), 7.91 (d, $J = 8.5$ Hz, 1H), 7.63 (dd, $J = 8.1, 5.1$ Hz, 2H), 7.43 (t, $J = 7.5$ Hz, 1H), 7.25 (d, $J = 8.5, 1\text{H}$). $^{13}\text{C-NMR}$: ($(\text{CD}_3)_2\text{SO}$, 100 MHz) 171.2, 166.3, 150.2, 148.8, 148.2, 144.7, 138.0, 135.0, 129.3, 128.1 (2C), 126.8, 123.9, 122.3, 120.1, 119.2, 108.9. HRMS (ESI, M^+) m/z calcd. for $\text{C}_{17}\text{H}_{13}\text{N}_3\text{O}_2$ 291.1002, found: 291.1006.

1-((*E*)-((*E*)-4-hydroxy-3-methoxybenzylidene)hydrazono)methyl)naphthalen-2-ol (3g)—Commercially obtained vanillin was reacted with anhydrous hydrazine as shown in General Method B, followed by condensation with 2-hydroxy-1-naphthaldehyde to obtain **3g**. Yield 0.70 g, 2.19 mmol; 44%. Yellow solid; mp 230 °C. IR: 3415 (secondary NH), 3300-3200 (broad, OH), 2150 (C=N), 1619 (C=O), 1577 (C=C), 1465 (C-H methyl), 1182 (C-O). $^1\text{H-NMR}$: (CDCl_3 , 500 MHz) δ 13.01 (s, 1H), 9.99 (s, 1H), 8.50 (s, 1H), 8.40 (s, 1H), 8.16 (d, $J = 8.5$ Hz, 1H), 8.05 (d, $J = 9.0$ Hz, 1H), 7.92 (d, $J = 8.0$ Hz, 1H), 7.85 (t, $J = 7.9$ Hz, 1H), 7.44 (t, $J = 7.4$ Hz, 1H), 7.34 (d, $J = 8.2$ Hz, 1H), 7.28 (t, $J = 9.0$ Hz, 1H), 7.19 (d, $J = 8.2$ Hz, 1H), 6.95 (d, $J = 8.6$ Hz, 1H), 3.97 (s, 3H). $^{13}\text{C-NMR}$: (CDCl_3 , 125 MHz) 170.8, 150.9, 149.4, 149.4, 135.0, 134.8, 129.3, 128.7, 128.1, 126.9, 124.6, 123.9, 122.9, 120.1, 119.2, 117.1, 114.3, 108.3, 56.1. HRMS (ESI, M^+) m/z calcd. for $\text{C}_{19}\text{H}_{16}\text{N}_2\text{O}_3$ 320.1155, found: 320.1157.

4-(dimethylamino)-*N'*-((2-hydroxynaphthalen-1-yl)methylene)benzohydrazide (3h)—

Commercially obtained *p*-(dimethylamino)benzaldehyde was reacted with anhydrous hydrazine as shown in General Method B, followed by condensation with 2-hydroxy-1-naphthaldehyde to obtain **3h**. Yield 1.28 g, 3.85 mmol; 77%. Orange solid; mp 231 °C. IR:

3500-3200 (broad, OH), 2901 (sp³ C-H), 2115 (C=N), 1629 (C=O), 1578 (C=C), 1319 (*N*, *N*-dimethyl), 1281 (C-N), 1241 (C-O). ¹H-NMR: (CDCl₃, 500 MHz) δ 13.56 (s, 1H), 9.69 (s, 1H), 8.61 (s, 1H), 8.21 (d, *J* = 8.5 Hz, 1H), 7.85 (d, *J* = 8.9 Hz, 1H), 7.8 (d, *J* = 8.9 Hz, 1H), 7.77 (d, *J* = 8.5 Hz, 1H), 7.57 (ddd, *J* = 8.4, 6.9, 1.4 Hz, 1H), 7.39 (ddd, *J* = 8.0, 6.9, 1.0 Hz, 1H), 7.26 (d, *J* = 9.0 Hz, 2H), 6.78 (d, *J* = 9.0 Hz, 2H), 3.10 (s, 6H). ¹³C-NMR: (CDCl₃, 125 MHz) 169.9, 159.0, 153.2, 150.8, 133.7, 132.1, 131.4 (2C), 129.1, 128.9, 127.6, 123.5, 121.4, 120.2, 119.2, 111.7 (2C), 108.2, 40.2 (2C). HRMS (ESI, M⁺) *m/z* calcd. for C₂₀H₁₉N₃O 318.1606, found: 318.1608.

***N'*-((2-hydroxynaphthalen-1-yl)methylene)-4-methoxybenzohydrazide (3i)—**

Commercially obtained *p*-anisaldehyde was reacted with anhydrous hydrazine as shown in General Method B, followed by condensation with 2-hydroxy-1-naphthaldehyde to obtain **3i**. Yield 1.43 g, 4.46 mmol; 89%. Yellow solid; mp 230 °C. IR: 3420 (secondary NH), 3300-3200 (broad, OH), 2113 (C=N), 1618 (C=O), 1577 (C=C), 1465 (C-H methyl), 1182 (C-O). ¹H-NMR: (CDCl₃, 500 MHz) δ 13.56 (s, 1H), 13.01 (s, 1H), 9.66 (s, 1H), 8.55 (s, 1H), 8.16 (d, *J* = 8.6 Hz, 1H), 7.79 (t, *J* = 9.3 Hz, 1H), 7.69 (d, *J* = 7.4 Hz, 2H), 7.59 (t, *J* = 7.6 Hz, 1H), 7.56 (t, 7.6 Hz, 1H), 7.38 (t, *J* = 7.4 Hz, 1H), 6.71 (d, *J* = 8.5 Hz, 2H), 3.06 (s, 3H). ¹³C-NMR: (CDCl₃, 125 MHz) 171.0, 161.1, 159.0, 135.0, 133.7, 130.4, 129.9, 129.3, 129.1, 128.1, 127.6, 123.9, 123.4, 120.2, 120.1, 119.2 (2C), 111.7, 50.2. HRMS (ESI, M⁺) *m/z* calcd. for C₁₉H₁₆N₂O₂ 304.1207, found: 304.1206.

***N'*-((2-hydroxynaphthalen-1-yl)methylene)-4-methylbenzohydrazide (3j)—**

Commercially obtained *p*-tolualdehyde was reacted with anhydrous hydrazine as shown in General Method B, followed by condensation with 2-hydroxy-1-naphthaldehyde to obtain **3j**. Yield 1.00 g, 3.29 mmol; 66% yield. Yellow solid; mp 228 °C. IR: 3300-3200 (broad, OH), 2113 (C=N), 1619 (C=O), 1577 (C=C), 1416 (C-C), 1281 (C-N), 1240 (C-O). ¹H-NMR: ((CD₃)₂SO, 400 MHz) δ 12.89 (br s, 1H), 9.98 (s, 1H), 8.64 (d, *J* = 8.3 Hz, 1H), 8.01 (t, *J* = 8.3 Hz, 1H), 7.90 (d, *J* = 8.0 Hz, 1H), 7.75 (d, *J* = 8.0 Hz, 2H), 7.60 (t, *J* = 7.6 Hz, 1H), 7.43 (t, *J* = 7.3 Hz, 1H), 7.36 (t, *J* = 7.3 Hz, 1H), 7.32 (d, *J* = 7.6 Hz, 2H), 7.25 (d, *J* = 7.3, 1H), 2.35 (s, 3H). ¹³C-NMR: (CDCl₃, 100 MHz) 169.7, 161.2, 149.9, 135.0, 132.6, 132.1, 129.7, 129.5, 129.3, 129.2, 129.1 (2C), 128.1, 123.9, 120.1, 119.2 (2C), 108.4, 21.4. HRMS (ESI, M⁺) *m/z* calcd. for C₁₉H₁₆N₂O 289.1341 found: 289.1353.

1-((2-benzylhydrazono)methyl)naphthalen-2-ol (3k)—Prepared according to general procedures described in the SI. Yield 1.24 g, 4.47 mmol; 89%. Yellow solid; mp 230 °C. IR: 3313 (secondary N-H), 3010 (sp² C-H), 2360 (C=N), 1618 (C=O), 1592 (C=C), 1467 (C-C), 1277 (C-N), 1253 (C-O). ¹H-NMR: ((CD₃)₂SO, 400 MHz) δ 11.84 (br s, 1H), 10.50 (s, 1H), 8.90 (s, 1H), 8.33 (d, *J* = 8.6 Hz, 1H), 7.85-7.82 (m, 2H), 7.53 (t, *J* = 7.9 Hz, 1H), 7.34 (t, *J* = 7.9 Hz, 1H), 7.30-7.21 (m, 5H), 7.17 (d, *J* = 8.9 Hz, 1H), 3.91 (s, 2H). ¹³C-NMR (CDCl₃, 100 MHz) 157.1, 143.6, 138.1, 131.6, 131.4, 129.8, 129.3, 128.6, 127.3, 123.5, 121.1, 120.1, 119.2, 112.9, 109.1, 58.7, 18.7. HRMS (ESI, M⁺) *m/z* calcd. for C₁₇H₁₆N₂O 262.1101 found: 262.1094.

1-((2-(4-bromophenyl)hydrazono)methyl)naphthalen-2-ol (3l)—Prepared according to general procedures described in the SI. Yield 1.23 g, 3.62 mmol; 72%. Yellow solid; mp

230 °C. IR: 3322 (secondary NH), 2118 (C=N), 1619 (C=O), 1589 (C=C), 1286 (C-N), 1251 (C-O), 650 (C-Br). ¹H-NMR: ((CD₃)₂SO, 400 MHz) δ 11.57 (br s, 1H), 10.64 (s, 1H), 8.89 (s, 1H), 8.45 (d, *J* = 8.5 Hz, 1H), 7.83 (d, *J* = 8.4 Hz, 1H), 7.78 (t, *J* = 7.3 Hz, 1H), 7.55 (t, *J* = 7.5 Hz, 1H), 7.40 (d, 8.1 Hz, 2H), 7.35 (t, *J* = 7.0 Hz, 1H), 7.16 (d, *J* = 8.9 Hz, 1H), 6.93 (d, *J* = 8.8 Hz, 2H). ¹³C-NMR (CDCl₃, 100 MHz) 160.1, 141.9, 138.7, 133.0, 132.4, 132.2, 132.1, 131.6, 129.2, 127.2, 126.6, 123.4, 119.8, 118.9, 118.8, 114.2 108.1. HRMS (ESI, M⁺) *m/z* calcd. for C₁₇H₁₃BrN₂O 340.0206, found 340.0207.

1-((2-(4-nitrophenyl)hydrazono)methyl)naphthalen-2-ol (3m)—Prepared according to general procedures described in the SI. Yield 1.23 g, 4.01 mmol; 80% yield. Red solid; mp 230 °C. IR: 3290 (secondary N-H), 2117 (C=N), 1589 (C=C), 1310 (C-O), 1267, 1296 (N-O). ¹H-NMR: ((CD₃)₂SO, 400 MHz) δ 11.41 (s, 1H), 11.14 (s, 1H), 8.98 (s, 1H), 8.75 (d, *J* = 8.6 Hz, 1H), 8.19 (d, *J* = 9.1 Hz, 2H), 7.86 (m, 2H), 7.60 (ddd, *J* = 8.4, 6.8, 1.3 Hz, 1H), 7.35 (m, 1H), 7.22 (d, *J* = 8.9 Hz, 1H), 7.11 (d, *J* = 8.9 Hz, 2H). ¹³C NMR: (CD₃CN, 100 MHz) 152.0, 148.6, 142.6, 134.1, 133.7, 132.8, 132.4, 129.0, 128.0, 126.6, 124.2 (2C), 120.8, 119.9, 111.6, 111.6, 108.4. HRMS (ESI, [M+Na]⁺) *m/z* calcd. for C₁₇H₁₃N₃O₃Na 330.0854, found: 330.0870.

2-hydroxy-*N'*-((5-hydroxy-1H-indol-3-yl)methylene)benzohydrazide (3n)—Prepared according to general procedures described in the SI. Yield 0.95 g, 3.21 mmol; 64% yield. Red solid. mp 230 °C. IR: 3290 (secondary N-H), 3300-3200 (broad, OH), 2117 (C=N), 1692 (C=O), 1589 (C=C), 1310 (C-O). ¹H NMR: (CD₃CN, 500 MHz): δ 11.21 (s, 1H), 11.04 (s, 1H), 10.50 (s, 1H), 9.71 (s, 1H), 8.60 (s, 1H), 7.89 (d, *J* = 8.6 Hz, 1H), 7.85 (d, *J* = 5.3 Hz, 1H), 7.64 (d, *J* = Hz, 1H), 7.46 (t, *J* = 6.8, 1H), 7.40 (d, *J* = 8.9 Hz, 1H), 6.99 (d, *J* = 8.9 Hz, 1H), 7.95 (t, *J* = 6.8 Hz, 1H), 6.92 (d, *J* = 5.4 Hz, 1H). ¹³C NMR: (CD₃CN, 125 MHz) 163.2, 157.1, 152.4, 146.2, 134.6, 130.4, 127.1, 125.1, 124.7, 124.2, 121.8, 118.3 (2C), 114.3, 114.2, 104.0. HRMS (ESI, M⁺) *m/z* calcd. for C₁₆H₁₃N₃O₃ 279.1002, found: 279.1006.

***N'*-((2-hydroxynaphthalen-1-yl)methylene)benzenesulfonohydrazide (3o)**—Commercially obtained benzene sulfonyl hydrazine was condensed with 2-hydroxy-1-naphthaldehyde as described in General Method D to obtain **3o**. Yield 1.47 g, 4.49 mmol; 89.8 %. Yellow solid; mp 230 °C. IR: 3156 (secondary N-H), 2117 (C=N), 1601 (C=C), 1309 (asymmetrical, S-O), 1074-972 (symmetrical, S-O), 683 (S-N), 638 (C-S). ¹H-NMR: : ((CD₃)₂SO, 400 MHz) δ 11.61 (s, 1H), 11.06 (s, 1H), 8.77 (s, 1H), 8.36 (d, *J* = 8.6 Hz, 1H), 7.92 (d, *J* = 7.0 Hz, 2H), 7.80 (d, *J* = 7.5 Hz, 1H), 7.76 (d, *J* = 7.0 Hz, 2H), 7.73-55 (m, 2H), 7.42 (ddd, *J* = 8.5, 6.8, 1.0 Hz, 1H), 7.33 (ddd, *J* = 8.0, 6.9, 1.0 Hz, 1H), 7.14 (d, *J* = 8.9 Hz, 1H). ¹³C-NMR: (CDCl₃, 100 MHz) 151.5, 143.2, 139.2, 134.2, 133.9, 133.9, 132.1, 129.5, 129.2, 129.2, 128.3, 128.0, 127.9, 123.8, 119.7, 119.0 108.9. HRMS (ESI, [M+Na]⁺) *m/z* calcd. for C₁₇H₁₄N₂O₃SNa 349.0623, found 349.0634.

***N'*-((2-hydroxynaphthalen-1-yl)methylene)-1-phenylmethanesulfonohydrazide (3p)**—Commercially obtained phenylmethyl-sulfonyl fluoride was reacted with anhydrous hydrazine as shown in General Method B, followed by condensation with 2-hydroxy-1-naphthaldehyde to obtain **3p**. Yield 0.31 g, 0.90 mmol; 18%. Yellow solid; mp 230 °C. IR:

3156 (secondary N-H), 2117 (C=N), 1601 (C=C), 1309 (asymmetrical, S-O). ¹H-NMR: ((CD₃)₂SO, 400 MHz) δ 12.84 (br s, 1H), 9.96 (s, 1H), 8.77 (s, 1H), 8.61 (d, *J* = 8.6 Hz, 1H), 7.99 (d, *J* = 8.4 Hz, 1H), 7.88 (d, *J* = 9.0 Hz, 1H), 7.58 (t, *J* = 8.5 Hz, 1H), 7.40 (t, *J* = 8.5 Hz, 1H), 7.36 (t, *J* = 8.5 Hz, 1H), 7.24 (m, 5H), 4.32 (s, 2H). ¹³C-NMR: (CDCl₃, 100 MHz) 150.5, 143.2, 139.2, 135.0, 133.8, 133.9, 132.1, 129.5, 129.3, 129.3, 128.3, 128.1, 127.9, 123.9, 120.1, 119.2, 108.9, 63.9. HRMS (ESI, [M+Na]⁺) *m/z* calcd. for C₁₈H₁₆N₂O₃SNa 363.0774, found: 363.0781.

***N'*-((2-hydroxynaphthalen-1-yl)methylene)-4-nitrobenzenesulfonohydrazide**

(3q)—Commercially obtained 4-nitrobenzenesulfonylhydrazine was reacted with anhydrous hydrazine as shown in General Method B, followed by condensation with 2-hydroxy-1-naphthaldehyde to obtain **3q**. Yield 1.59 g, 4.29 mmol; 86%. Yellow solid; mp 230 °C. IR: 3311 (secondary N-H), 2116 (C=N), 1577 (C=C), 1280 (C-N), 1240 (C-O), 953-869 (S-O), 679 (S-N), 657 (C-S). ¹H-NMR: ((CD₃)₂SO, 500 MHz) δ 11.02 (s, 1H), 9.98 (s, 1H), 8.77 (s, 1H), 8.64 (d, *J* = 8.6 Hz, 2H), 8.19 (d, *J* = 8.4 Hz, 1H), 8.02 (d, *J* = 9.0 Hz, 2H), 7.91 (d, *J* = 8.1 Hz, 1H), 7.85 (t, *J* = 8.1 Hz, 1H), 7.61 (t, *J* = 8.0 Hz, 1H), 7.43 (t, *J* = 7.5 Hz, 1H), 7.27 (d, *J* = 8.9 Hz, 1H). ¹³C-NMR: (CDCl₃, 125 MHz) 157.2, 151.7, 150.9, 147.4, 136.0, 133.7, 129.3, 128.5 (2C), 128.1, 126.1, 124.2, 123.9, 123.9, 120.1, 119.7, 118.5. HRMS (ESI, [M+Na]⁺) *m/z* calcd. for C₁₇H₁₃N₃O₅SNa 393.0468, found: 393.0474.

***N'*-((2-hydroxynaphthalen-1-yl)methylene)-4-methylbenzenesulfonohydrazide**

(3r)—Commercially obtained *d*-10 camphoresulfonic acid was converted to its ethyl ester as shown in General Method A (see SI). General methods B and D (see SI) were then followed as previously described to obtain **3r**. Yield 0.55 g, 1.63 mmol; 33%. Yellow solid; mp 230 °C. IR: 2117 (C=N), 1680 (C=O), 1577 (C=C), 1465 (C-C), 1318-1281 (N-O), 1240 (C-O), 679 (S-N), 656 (C-S). ¹H-NMR: ((CD₃)₂SO, 400 MHz) δ 12.67 (s, 1H), 9.99 (s, 1H), 8.70 (s, 1H), 8.03 (d, *J* = 9.0 Hz, 1H), 7.91 (d, *J* = 8.1 Hz, 1H), 7.61 (t, *J* = 7.6 Hz, 1H), 7.49-7.39 (m, 1H), 7.29 (dd, *J* = 14.1, 8.4 Hz, 1H), 7.12-7.05 (m, 1H), 3.38 (d, *J* = 15.1 Hz, 1H), 3.04 (d, *J* = 15.1 Hz, 1H), 2.52 (dd, *J* = 4.9, 2.7 Hz, 1H), 2.16 (t, *J* = 4.6 Hz, 1H), 2.15-1.99 (m, ³H), 1.44 (d, *J* = 8.7, 3.8 Hz, 1H), 0.93 (d, *J* = 9.3 Hz, 6H). ¹³C-NMR: ((CD₃)₂SO, 100 MHz) 144.9, 135.0, 129.3, 128.5, 124.2, 122.4, 119.2, 119.0, 53.6, 53.2, 49.7, 49.4, 48.4, 35.3, 28.3, 27.4, 20.6, 19.8, 18.1, 18.0, 15.4. HRMS (ESI, [M+Na]⁺) *m/z* calcd. for C₂₁H₂₄N₂O₄SNa 423.1349, found: 423.1358.

4-amino-3-chloro-*N'*-((2-hydroxynaphthalen-1-yl)methylene)benzohydrazide

(3s)—Commercially obtained *p*-toluenesulfonylhydrazine was condensed with 2-hydroxy-1-naphthaldehyde as described in General Method D (see SI) to obtain **3s**. Yield 0.85 g, 2.51 mmol; 50%. Yellow solid; mp 230 °C. IR: 3163 (secondary N-H), 3036 (aromatic C-H), 2104 (C=N), 1620 (primary NH₂), 1578 (C=C), 1281 (C-N), 1241 (C-O), 666 (C-Cl). ¹H-NMR: (CDCl₃, 500 MHz) δ 12.18 (s, 1H), 10.81 (s, 1H), 9.67 (s, 1H), 8.16 (d, *J* = 8.5 Hz, 1H), 7.97 (t, *J* = 8.5 Hz, 1H), 7.88 (d, *J* = 9.0 Hz, 2H), 7.80 (t, *J* = 9.7 Hz, 1H), 7.59 (t, *J* = 7.5 Hz, 1H), 7.40 (t, *J* = 7.5 Hz, 1H), 7.20 (d, *J* = 9.0 Hz, 2H), 7.13 (d, *J* = 9.7 Hz, 1H), 2.39 (s, 3H). ¹³C-NMR: (CDCl₃, 125 MHz) 150.9, 143.3, 143.2, 135.0, 133.8, 132.8, 129.7, 129.5, 129.3, 128.3, 128.1, 126.6, 123.9, 120.1, 119.2, 118.5, 108.9, 30.7. HRMS (ESI, [M+Na]⁺) *m/z* calcd. for C₁₈H₁₆N₂O₃SNa 363.0774, found: 363.0771.

3-chloro-*N'*-((2-hydroxynaphthalen-1-yl)methylene)-4-nitrobenzohydrazide (3t)

—Prepared according to general procedures described in the SI. Yield 1.36 g, 3.69 mmol; 74%. Orange solid; mp 230 °C. IR: 3415 (secondary NH), 3300-3200 (broad, OH), 2117 (C=N), 1618 (C=O), 1577 (C=C), 1318 1280 (symmetrical N-O), 1182 (C-O), 721 (C-Cl). ¹H NMR: (CDCl₃, 500 MHz) δ 13.01 (s, 1H), 9.67 (s, 1H), 8.16 (d, *J* = 8.5 Hz, 1H), 7.88 (d, *J* = 9.0 Hz, 1H), 7.80 (dd, *J* = 8.1, 1.4 Hz, 2H), 7.66-7.55 (m, 2H), 7.40 (ddd, *J* = 8.0, 6.8, 1.0 Hz, 2H), 7.25 (d, *J* = 9.0 Hz, 1H) 7.17 (d, *J* = 9.0 Hz, 1H), 2.5 (s, 2H). ¹³C NMR: (CDCl₃, 125 MHz) 169.5, 163.4, 147.8, 143.0, 135.0, 133.3, 129.3, 128.1 (2C), 127.8, 125.5, 125.4, 123.9, 120.1, 119.7, 119.1, 118.9, 118.6. HRMS (ESI, M⁺) *m/z* calcd. For C₁₈H₁₄ClN₃O₂ 339.0055, found 339.0059.

5-bromo-*N'*-((2-hydroxynaphthalen-1-yl)methylene)-2-methoxybenzohydrazide (3u)

—Prepared according to general procedures described in the SI. Yield 1.25 g, 3.14 mmol; 63%. Yellow solid; mp 229 °C. IR: 3272 (secondary N-H), 3171 (sp² C-H), 2996 (sp³ C-H), 2094 (C=N), 1639 (C=O), 1550 (C=C), 1235 (C-O), 635 (C-Br). ¹H-NMR: (C₂D₆SO, 400 MHz) δ 12.76 (s, 1H), 11.76 (s, 1H), 9.43 (s, 1H), 8.25 (d, *J* = 8.6 Hz, 1H), 7.92 (d, *J* = 8.5 Hz, 1H), 7.88 (d, *J* = 9.0 Hz, 1H), 7.68 (d, *J* = 8.1 Hz, 1H), 7.58 (ddd, *J* = 8.4, 6.9, 1.3 Hz, 1H), 7.44-7.27 (m, ³H), 7.22 (d, *J* = 9.0 Hz, 1H). ¹³C-NMR: (CDCl₃, 100 MHz) 168.4, 164.1, 151.0, 143.1, 143.0, 135.0, 133.3, 129.7, 129.5, 124.1, 129.3, 128.1, 127.8, 123.9, 120.1, 119.7, 119.2, 118.9. HRMS (ESI, [M+Na]⁺) *m/z* calcd. for C₁₈H₁₂ClN₃O₄Na 369.0511, found: 363.0516.

5-bromo-*N'*-((2-hydroxynaphthalen-1-yl)methylene)-2-methoxybenzohydrazide (3v)

—Prepared according to general procedures described in the SI. Yield 1.70 g, 4.26 mmol; 85%. Yellow solid; mp 230 °C. IR: 3273 (secondary N-H), 2116 (C=N), 1642 (C=O), 1583 (C=C), 1462 (C-C), 1233 (C-O), 648 (C-Br). ¹H-NMR: (CD₃CN, 500 MHz) δ 13.07 (br s, 1H), 11.11 (s, 1H), 9.47 (s, 1H), 8.29 (d, *J* = 8.5 Hz, 1H), 8.13 (d, *J* = 8.4 Hz, 1H), 8.00 (m, 1H), 7.96 (m, 1H), 7.70 (ddd, *J* = 8.5, 6.9, 1.4 Hz, 1H), 7.55-7.48 (m, 2H), 7.42 (dd, *J* = 8.4, 1.8 Hz, 1H), 7.32 (d, *J* = 9.0 Hz, 1H) 4.21 (s, 3H). ¹³C NMR (CD₃CN, 125 MHz) 161.3, 159.2, 157.3, 148.3, 134.1, 133.8, 129.8, 128.5, 128.5, 125.3, 124.5, 121.2, 120.0, 119.5, 116.5, 114.9, 112.7, 109.4, 30.8. HRMS (ESI, M⁺) *m/z* calcd. for C₁₉H₁₅BrN₂O₃ 421.0164, found 421.0164.

4-bromo-*N'*-((2-hydroxynaphthalen-1-yl)methylene)-2-methoxybenzohydrazide (3w)

—Prepared according to general procedures described in the SI. Yield 1.70 g, 4.26 mmol; 85%. Yellow solid; mp 230 °C. IR: 3273 (secondary N-H), 2116 (C=N), 1642 (C=O), 1583 (C=C), 1462 (C-C), 1233 (C-O), 648 (C-Br). ¹H-NMR: (CD₃CN, 500 MHz) δ 13.07 (br s, 1H), 11.11 (s, 1H), 9.47 (s, 1H), 8.29 (d, *J* = 8.5 Hz, 1H), 8.13 (d, *J* = 8.4 Hz, 1H), 8.00 (m, 1H), 7.96 (m, 1H), 7.70 (ddd, *J* = 8.5, 6.9, 1.4 Hz, 1H), 7.55-7.48 (m, 2H), 7.42 (dd, *J* = 8.4, 1.8 Hz, 1H), 7.32 (d, *J* = 9.0 Hz, 1H) 4.21 (s, 3H). ¹³C NMR (CD₃CN, 125 MHz) 161.5, 160.1, 157.4, 148.3, 134.1, 133.8, 129.8, 128.5, 125.3, 124.5, 121.2, 120.0, 119.4, 118.7, 116.5, 114.3, 112.4, 109.1, 30.8. HRMS (ESI, M⁺) *m/z* calcd. For C₁₉H₁₅BrN₂O₃ 421.0164, found 421.0174.

Benzyl2-((2-hydroxynaphthalen-1-yl)methylene)hydrazine-1-carboxylate (3x)—

Prepared according to general procedures described in the SI. Yield 0.25 g, 0.78 mmol; 16%. Yellow solid; mp 230 °C. IR: 2987 (sp³ C-H), 2117 (C=N), 1694 (ester C=O), 1578 (C=C), 1467 (C-C), 1281 (C-N), 1239 (C-O). ¹H-NMR: (CD₃CN, 500 MHz) δ 12.46 (s, 1H), 9.52 (br. s, 1H), 9.11 (s, 1H), 8.12 (d, *J* = 8.6 Hz, 1H), 7.98-7.91 (m, 2H), 7.66 (ddd, *J* = 8.5, 6.9, 1.4 Hz, 1H), 7.60 – 7.43 (m, 5H), 7.27 (d, *J* = 9.0 Hz, 1H), 7.17 (d, *J* = 8.9 Hz, 1H), 5.35 (s, 2 H). ¹³C-NMR (CD₃CN, 125 MHz) 165.2, 153.5, 143.6, 133.3, 132.9, 129.8, 129.5 (2C), 129.1, 128.9, 128.5 (2C), 128.0, 127.9, 124.5, 120.9, 119.7, 108.9, 67.8. HRMS (ESI, [M +Na]⁺) *m/z* calcd. for C₁₉H₁₆N₂O₃Na 343.1059, found 343.1049.

2-hydroxy-*N*'-((7-methyl-1H-indol-3-yl)methylene)benzo-hydrazide (3z)—

Prepared according to general procedures described in the SI. Yield 0.21 g, 0.73 mmol; 15%. Yellow solid. mp 230 °C. IR: 3300-3200 (broad, OH), 2987 (sp³ C-H), 2117 (C=N), 1694 (C=O), 1578 (C=C), 1467 (C-C), 1281 (C-N), 1239 (C-O). ¹H-NMR: (CD₃CN, 500 MHz) δ 12.36 (s, 1H), 11.04 (s, 1H), 9.80 (br. s, 1H), 8.57 (s, 1H), 8.18 (d, *J* = 8.6 Hz, 1H), 7.79 (d, *J* = 5.5 Hz, 1H), 7.71 (d, *J* = 6.9 Hz, 1H), 7.49 (t, *J* = 9.1 Hz, 1H), 7.18 (t, *J* = 9.0 Hz, 1H), 7.12 (d, *J* = 8.9 Hz, 1H), 7.00 (d, *J* = 6.8 Hz, 1H), 6.96 (d, *J* = 5.4 Hz, 1H), 2.55 (s, 3H). ¹³C-NMR (CD₃CN, 125 MHz) 163.0, 161.2, 146.2, 134.6, 132.3, 130.4, 127.1, 126.0, 124.4, 124.2, 121.8, 120.0, 119.1, 118.3, 118.2, 109.5, 16.2. HRMS (ESI, M⁺) *m/z* calcd. for C₁₇H₁₅N₃O₂ 293.1159, found: 293.1162.

Growth Inhibitory Assays against Cancer Cell lines

Growth inhibition assays to assess cellular toxicity were performed in the Case Comprehensive Cancer Center, CWRU, in a manner similar to recently reported data.¹⁰ Human colon cancer (HCT116) and human breast cancer (MDA-MB-231) cell lines were maintained in standard growth media consisting of (RPMI1640 + 10% FBS + 2 mM glutamine + 100 U/mL penicillin, 100 µg/mL streptomycin). Cell growth was monitored and shown to be negative for mycoplasma contamination using the Mycoplasma Detection kit (MycoAlert™, Lonza, Basel, Switzerland). For growth inhibition assays, cells were harvested by trypsinization and seeded into 96-well tissue culture plates at 2500 cells/mL. The following day an equal volume of 2x-inhibitor containing medium was added to each well. The cells were cultured for 3 additional days at 37 °C in a 5% CO₂ humidified incubator. HCT-116 and MDA-MB-231 cell lines were treated with inhibitor concentrations of 10.0, 1.0, and 0.1 µM respectively. Cell growth (and its inhibition) was assessed by measuring total DNA content per well using the method of Labarca and Paigen²³ and reported as cellular IC₅₀ values. Results of this evaluation are presented in Table S2 (see SI).

Sensitization of MDA-MB-231 cell line toward NSAH inhibitor under siRNA transfection and RRM1 knockdown conditions

All reagents necessary to perform siRNA transfection and knockdown studies were purchased from ThermoFisher, Grand Island, NY, unless otherwise noted. siRNA transfection was performed using the Lipofectamine[®] 2000 reagent per manufacturer's instructions. siRNA pools (RRM1 Silencer[®] Select, 3 RefSeqs; or control scrambled siRNA) at 0–50 pmole/well concentrations, were diluted in serum-free Opti-MEM media, then mixed with Lipofectamine[®] 2000 to allow formation of respective complexes. This solution

was then serially diluted in Opti-MEM media and pipetted into wells of a standard 96-well tissue culture plate. An equal number of MDA-MB-231 breast cancer cells (1000/well) diluted in RPMI1640 + 10% FBS (without antibiotics) and were then added to each well and cells were incubated for 48 hours at 37 °C in a 5% CO₂ humidified tissue culture incubator to allow for repression of RRM1. Specific inhibitor **3a** was then added as 5X concentrated stock, diluted in cell culture media, and cells were allowed to grow for an additional 5 days. Each series of siRNAs (0, 0.25, 0.5, 1.0, 2.0 & 4.0 pmole/well) were treated with a dose range of **3a** in duplicate (20 μM to 0.075 μM, with an additional inhibitor-free control; in 2-fold dilution increment). DNA concentration was then measured using an adaptation of the method of Labarca and Paigen.²³ Media was removed, cells washed briefly in 0.25X PBS, followed by addition of 100 μL of ddH₂O water to each well. The plates were subjected to a cycle of freezing and thawing to induce hypotonic lysis. DNA dye (Hoechst 33258, bisbenzamide, Sigma Aldrich, St. Louis, MO) diluted in 2M NaCl, 10 mM Tris-HCl, pH 7.4 was then added to each well and allowed to incubate in the dark at room temperature for 2 hours. Intensity in the wells in each Plate was then read using a SpectraMax i3 fluorescence plate reader (Molecular Devices, Sunnyvale, CA) using excitation/emission wavelengths of 370/460 nm, respectively. A standard curve using purified salmon DNA was included to allow for determination of DNA amounts per well. Cell growth inhibition is calculated relative to untreated controls; individual curves were generated for each siRNA amount.

Supplementary Material

Refer to Web version on PubMed Central for supplementary material.

Acknowledgments

Authors thank Dr. William E. Harte (School of Medicine, CWRU) for insightful comments and suggestions during the development of this project. Authors thank Tyler Jenkins for synthesis of aldehyde precursor involved in the synthesis of **3c**. The authors thank Dr. Johnathon Karty and Angela Hansen from Indiana University for providing high resolution mass spectrometry analysis on all analogs. The authors thank the Univ. of Cincinnati library (former P&G library), and specifically Dr. William Seibel, for providing access to the high throughput screening library.

Funding Sources

This study is partly funded by NIH funding to PI: Dr. Chris G. Dealwis (R01GM100887). RV thanks the Department of Chemistry for funding portions of this project. The authors thank the National Science Foundation for major research instrumentation funding through the grant to the Department of Chemistry (NSF MRI-1334048). This research was supported in part by the Translational Research Shared Resource of the Case Comprehensive Cancer Center (P30 CA043703). The authors acknowledge these funding sources for their support.

Abbreviations

ADP	adenosine diphosphate
Anhyd.	anhydrous
ATP	adenosine triphosphate
CDCl₃	chloroform-d
CD₃CN	acetonitrile-d

(CD₃)OD	dimethylsulfoxide-d
DEPT	distortionless enhancement by polarization transfer
DMF	dimethylformamide
DMSO	dimethylsulfoxide
DTT	dithiothreitol
EDTA	ethylenediaminetetraacetic acid
GTP	guanosine triphosphate
HEPES	4-(2-hydroxyethyl)-1-piperazineethanesulfonic acid
HPLC	high performance liquid chromatography
HRMS	high resolution mass spectrometry
hRRM1	human ribonucleotide reductase mammalian 1
hRRM2	human ribonucleotide reductase mammalian 2
H₂SO₄	sulfuric acid
IC₅₀	half maximal inhibitory concentration
IR	infrared
LiAlH₄	lithium aluminum hydride
MeOH	methanol
MHz	megahertz
MP	melting point
NaHCO₃	sodium bicarbonate
NaOH	sodium hydroxide
NMR	nuclear magnetic resonance
PCC	pyridinium chlorochromate
RR	ribonucleotide reductase
siRNA	small interfering RNA
TLC	thin layer chromatography
UV	ultraviolet

References

- (a) Brown NC, Reichard P. Role of effector binding in allosteric control of ribonucleoside diphosphate reductase. *J. Mol. Biol.* 1969; 46:39–55. [PubMed: 4902212] (b) Thelander L, Reichard P. Reduction of ribonucleotides. *Annu. Rev. Biochem.* 1979; 48:133–158. [PubMed: 382982] (c) Eriksson M, Uhlin U, Ramaswamy S, Ekberg M, Regnström K, Sjöberg BM, Eklund H. Binding of allosteric effectors to ribonucleotide reductase protein R1: reduction of active-site cysteines promotes substrate binding. *Structure.* 1997; 5:1077–1092. [PubMed: 9309223] (d) Larsson KM, Jordan A, Eliasson R, Reichard P, Logan DT, Nordlund P. Structural mechanism of allosteric substrate specificity regulation in a ribonucleotide reductase. *Nat. Struct. Mol. Biol.* 2004; 11:1142–1149. [PubMed: 15475969] (e) Xu H, Faber C, Uchiki T, Fairman JW, Racca J, Dealwis CG. Structures of eukaryotic ribonucleotide reductase I provide insights into dNTP regulation. *Proc. Natl. Acad. Sci.* 2006; 103:4022–4027. [PubMed: 16537479] (f) Wang J, Lohman GJ, Stubbe J. Enhanced subunit interactions with gemcitabine-5'-diphosphate inhibit ribonucleotide reductases. *Proc. Natl. Acad. Sci.* 2007; 104:14324–14329. [PubMed: 17726094] (g) Kashlan OB, Cooperman BS. Comprehensive model for allosteric regulation of mammalian ribonucleotide reductase: refinements and consequences. *Biochemistry.* 2003; 42:1696–1706. [PubMed: 12578384]
- (a) Rosell R, Crino L, Danenberg K, Scagliotti G, Bepler G, Taron M, Alberola V, Provencio M, Camps C, De MF, Sanchez JJ, Penas R. Targeted therapy in combination with gemcitabine in non-small cell lung cancer. *Semin. Oncol.* 2003; 30:19–25. (b) Rosell R, Fossella F, Milas L. Molecular markers and targeted therapy with novel agents: prospects in the treatment of non-small cell lung cancer. *Lung Cancer.* 2002; 38:43–49. (c) Rosell R, Taron M, Sanchez JM, Moran T, Reguart N, Besse B, Isla D, Massuti B, Alberola V, Sanchez JJ. The promise of pharmacogenomics: gemcitabine and pemetrexed. *Oncology.* 2004; 18:70–76. [PubMed: 15655942]
- (a) Knappenberger AJ, Ahmad MF, Viswathanan R, Dealwis CG, Harris ME. Nucleotide analog triphosphates allosterically regulate human ribonucleotide reductase and identify chemical determinants that drive substrate specificity. *Biochemistry.* 2016; 55:5884–5896. [PubMed: 27634056] (b) Fu Y, Lin H, Wisitpitthaya S, Blessing WA, Aye Y. A fluorometric readout reporting the kinetics of nucleotide-induced human ribonucleotide reductase oligomerization. *ChemBioChem.* 2014; 15:2598–2604. [PubMed: 25256246] (c) Rofougaran R, Vodnala M, Hofer A. Enzymatically active mammalian ribonucleotide reductase exists primarily as an $\alpha_6\beta_2$ octamer. *J. Biol. Chem.* 2006; 281:27705–27711. [PubMed: 16861739]
- (a) Ando N, Brignole EJ, Zimanyi CM, Funk MA, Yokoyama K, Asturias FJ, Stubbe J, Drennan CL. Structural interconversions modulate activity of *Escherichia coli* ribonucleotide reductase. *Proc. Natl. Acad. Sci. U.S.A.* 2011; 108:21046–21051. [PubMed: 22160671] (b) Ando N, Li H, Brignole EJ, Thompson S, McLaughlin MI, Page JE, Asturias FJ, Stubbe J, Drennan CL. Allosteric inhibition of human ribonucleotide reductase by dATP entails the stabilization of a hexamer. *Biochemistry.* 2016; 55:373–381. [PubMed: 26727048] (c) Zimanyi CM, Chen PYT, Kang G, Funk MA, Drennan CL. Molecular basis for allosteric specificity regulation in class IA ribonucleotide reductase from *Escherichia coli*. *eLife.* 2016; 5:e07141. [PubMed: 26754917] (d) Wisitpitthaya S, Zhao Y, Long MJ, Li M, Fletcher EA, Blessing WA, Weiss RS, Aye Y. Cladribine and fludarabine nucleotides induce distinct hexamers defining a common mode of reversible RNR inhibition. *ACS Chem. Biol.* 2016; 11:2021–2032. [PubMed: 27159113]
- (a) Ahmad, MF., Dealwis, CG. The structural basis for the allosteric regulation of ribonucleotide reductase. In: Giraldo, J., Ciruela, F., editors. *Oligomerization in Health and Disease*. Vol. 117. Academic Press; Cambridge, MA: 2013. p. 389-410. (b) Cooperman, BS., Dealwis, CG. Allosteric regulation and inhibition of class 1a ribonucleotide reductase activity. In: Anderson, K., editor. *Ribonucleotide Reductase*. Nova Science Publishers, Inc; Hauppauge, NY: 2008. p. 99-124. (c) Fairman JW, Wijerathna SR, Ahmad MF, Xu H, Nakano R, Jha S, Prendergast J, Welin RM, Flodin S, Roos A, Nordlund P, Li Z, Walz T, Dealwis CG. Structural basis for allosteric regulation of human ribonucleotide reductase by nucleotide-induced oligomerization. *Nat. Struct. Mol. Biol.* 2011; 18:316–322. [PubMed: 21336276] (d) Xu H, Fairman JW, Wijerathna SR, Kreisler NR, LaMacchia J, Helmbrecht E, Cooperman BS, Dealwis CG. The structural basis for peptidomimetic inhibition of eukaryotic ribonucleotide reductase: A conformationally flexible pharmacophore. *J. Med. Chem.* 2008; 51:4653–4659. [PubMed: 18610997] (e) Aye Y, Li M, Long MJ, Weiss RS.

Ribonucleotide reductase and cancer: biological mechanisms and targeted therapies. *Oncogene*. 2015; 34:2011–2021. [PubMed: 24909171]

6. (a) Heinemann V, Schulz L, Issels RD, Plunkett W. Gemcitabine: a modulator of intracellular nucleotide and deoxynucleotide metabolism. *Semin. Oncol.* 1995; 22:11–18. (b) Baker CH, Banzon J, Bollinger JM, Stubbe J, Samano V, Robin MJ, Lippert B, Jarvi E, Resvick R. 2'-Deoxy-2'-methylene-cytidine and 2'-deoxy-2',2'-difluorocytidine 5'-diphosphates: potent mechanism-based inhibitors of ribonucleotide reductase. *J. Med. Chem.* 1991; 34:1879–1884. [PubMed: 2061926] (c) Wang J, Lohman GJ, Stubbe J. Mechanism of inactivation of human ribonucleotide reductase with p53R2 by gemcitabine 5'-diphosphate. *Biochemistry*. 2009; 48:11612–11621. [PubMed: 19899807] (d) Plunkett W, Huang P, Gandhi V. Preclinical characteristics of gemcitabine. *Anticancer Drugs*. 1995; 6:7–13.
7. (a) Heinemann V, Xu YZ, Chubb S, Sen A, Hertel LW, Grindey GB, Plunkett W. Cellular elimination of 2',2'-difluorodeoxycytidine 5'-triphosphate: a mechanism of self-potentialiation. *Cancer Res.* 1992; 52:533–539. [PubMed: 1732039] (b) Huang P, Plunkett W. Phosphorolytic cleavage of 2-fluoroadenine from 9- β -D-arabinofuranosyl-2-fluoroadenine by *Escherichia coli*: A pathway for 2-fluoro-ATP production. *Biochem. Pharmacol.* 1987; 36:2945–2950. [PubMed: 3307790] (c) Gandhi V, Plunkett W. Modulatory activity of 2',2'-difluorodeoxycytidine on the phosphorylation and cytotoxicity of arabinosyl nucleosides. *Cancer Res.* 1990; 50:3675–3680. [PubMed: 2340517] (d) Gandhi V, Huang P, Xu YZ, Heinemann V, Plunkett W. Metabolism and action of 2',2'-difluorodeoxycytidine: self-potentialiation of cytotoxicity. *Adv. Exp. Med. Biol.* 1991; 309:125–130.
8. Ahmad MF, Huff SE, Pink J, Alam I, Zhang A, Perry K, Harris ME, Misko T, Porwal SK, Oleinick NL, Miyagi M, Viswanathan R, Dealwis CG. Identification of non-nucleoside human ribonucleotide reductase modulators. *J. Med. Chem.* 2015; 58:9498–9509. [PubMed: 26488902]
9. Dealwis, CG. Method of modulating ribonucleotide reductase. U.S. Patent 2015. 009,4314A1. Apr 2. 2015
10. Ahmad MF, Alam I, Huff SE, Pink J, Flanagan S, Shewach DS, Misko TA, Oleinick NL, Harte W, Viswanathan R, Harris ME, Dealwis CG. Potent competitive inhibition of human ribonucleotide reductase by a non-nucleoside small molecule. *Proc. Natl. Acad. Sci. U.S.A.* 2017; 114:8241–8246. [PubMed: 28716944]
11. (a) Baell JB, Holloway GA. New substructure filters for removal of pan assay interference compounds (PAINS) from screening libraries and for their exclusion in bioassays. *J. Med. Chem.* 2010; 53:2719–2740. [PubMed: 20131845] (b) Baell JB, Ferrins L, Falk H, Nikolakopoulos G. PAINS: Relevance to tool compound discovery and fragment-based screening. *Australian J. Chem.* 2013; 66:1483–1494. (c) Whitty A. Growing PAINS in academic drug discovery. *Future Med. Chem.* 2011; 3:797–801. [PubMed: 21644825] (d) Aldrich C, Bertozzi C, Georg GI, Kiessling L, Lindsley C, Liotta D, Merz KM, Schepartz A, Wang S. The ecstasy and agony of assay interference compounds. *ACS Central Sci.* 2017; 3:143–147.
12. van Dijken DJ, Kovaricek P, Ihrig SP, Hecht S. Acylhydrazones as widely tunable photoswitches. *J. Am. Chem. Soc.* 2015; 137:14982–14991. [PubMed: 26580808]
13. (a) Lepoivre M, Flaman JM, Bobe P, Lemaire G, Henry Y. Quenching of the tyrosyl free radical of ribonucleotide reductase by nitric oxide: relationship to cytostasis induced in tumor cells by cytotoxic macrophages. *J. Biol. Chem.* 1994; 269:21891–21897. [PubMed: 7520445] (b) Szalai VA, Brudvig GW. Reversible binding of nitric oxide to tyrosyl radicals in photosystem II: Nitric oxide quenches formation of the S3 EPR signal species in acetate-inhibited photosystem II. *Biochemistry*. 1996; 35:15080–15087. [PubMed: 8942675]
14. Heinemann V, Plunkett W. Modulation of deoxynucleotide metabolism by the deoxycytidylate deaminase inhibitor 3,4,5,6-tetrahydrodeoxyuridine. *Biochem. Pharmacol.* 1989; 38:4115–21. [PubMed: 2688654]
15. (a) Nyholm S, Mann GJ, Johansson AG, Bergeron RJ, Graeslund A, Thelander L. Role of ribonucleotide reductase in inhibition of mammalian cell growth by potent iron chelators. *J. Biol. Chem.* 1993; 268:26200–26205. [PubMed: 8253740] (b) Hershko C. Control of disease by selective iron depletion: a novel therapeutic strategy utilizing iron chelators. *Baillieres Clin. Haematol.* 1994; 7:965–1000. [PubMed: 7881162] (c) Lundberg JH, Chitambar CR. Interaction of gallium nitrate with fludarabine and iron chelators: effects on the proliferation of human leukemic HL60 cells. *Cancer Res.* 1990; 50:6466–6470. [PubMed: 1698536] (d) Mescher AL, Munaim SI. Transferrin and the growth-promoting effect of nerves. *Int. Rev. Cytol.* 1988; 110:1–26. [PubMed:

- 3053497] (e) Nocentini G, Federici F, Franchetti P, Barzi A. 2,2'-bipyridyl-6-carbothioamide and its ferrous complex: Their *in vitro* antitumoral activity related to the inhibition of ribonucleotide reductase R2 subunit. *Cancer Res.* 1993; 53:19–26. [PubMed: 8416745]
16. (a) Bianchi V, Pontis E, Reichard P. Changes of deoxyribonucleoside triphosphate pools induced by hydroxyurea and their relation to DNA synthesis. *J. Biol. Chem.* 1986; 261:16037–16042. [PubMed: 3536919] (b) Lagergren J, Reichard P. Purine deoxyribonucleosides counteract effects of hydroxyurea on deoxyribonucleoside triphosphate pools and DNA synthesis. *Biochem. Pharmacol.* 1987; 36:2985–2991. [PubMed: 3498491]
17. Reid G, Wallant NC, Patel R, Antonic A, Saxon-Aliifaalogo F, Cao H, Webster G, Watson JD. Potent subunit-specific effects on cell growth and drug sensitivity from optimized siRNA-mediated silencing of ribonucleotide reductase. *J. RNAi Gene Silencing.* 2009; 5:321–330. [PubMed: 19771229]
18. (a) Cohen, FE., McKerrow, JH., Ring, CS., Rosenthal, PJ., Kenyon, GL., Li, Z. Preparation of Hydrazides as Inhibitors of Metazoan Parasite Proteases. U.S. Patent. 5610192A. Mar 11. 1997 (b) Cohen, FE., McKerrow, JH., Ring, CSY., Rosenthal, PJ., Kenyon, GL., Li, Z. Inhibitors of Metazoan Parasite Proteases. WO 9406280A1. Mar 31. 1994
19. Munoz DL, Cardona DP, Cardona A, Carrillo LM, Quinones W, Echeverri F, Velez ID, Robledo SM. Effect of hydrazones against intracellular amastigotes of *Leishmania panamensis* and a parasitic cysteine protease. *Vitae.* 2006; 13:5–12.
20. Drewes, MW., Haug, M., Luerssen, K., Santel, HJ., Schmidt, RR. Herbicidal naphthalene Derivatives: Preparation of 2-(4,6-dimethoxypyrimidin-2-yloxy)-1-naphthaldehyde Hydrazones as Herbicides. U.S. Patent. 07/680,495. Feb 9. 1993
21. (a) Tan Z, Wortman M, Dillehay KL, Seibel WL, Evelyn CR, Smith SJ, Malkas LH, Zheng Y, Lu S, Dong Z. Small-molecule targeting of proliferating cell nuclear antigen chromatin association inhibits tumor cell growth. *Mol. Pharmacol.* 2012; 81:811–819. [PubMed: 22399488] (b) Dillehay KL, Seibel WL, Zhao D, Lu S, Dong Z. Target validation and structure-activity analysis of a series of novel PCNA inhibitors. *Pharmacol. Res. Perspect.* 2015; 3:1–14. (c) Dong, Z., Wortman, M., Tan, Z., Dillehay, K. Methods for Identification of Proliferating Cell Nuclear Antigen (PCNA) Targeting Compounds for Cancer Therapy and PCNA Function Regulation. WO2012033938A2. Mar 15. 2012
22. Flanagan SA, Robinson BW, Krokosky CM, Shewach DS. Mismatched nucleotides as the lesions responsible for radiosensitization with gemcitabine: a new paradigm for antimetabolite radiosensitizers. *Mol. Cancer Ther.* 2007; 6:1858–1868. [PubMed: 17575114] (b) In a personal communication, Dr. Shewach further reaffirmed their view of NSAH inhibiting hRR to cause perturbations in cellular dNTP levels leading to results published earlier (reference 10).
23. Labarca C, Paigen KA. Simple, rapid, and sensitive DNA assay procedure. *Anal. Biochem.* 1980; 102:344–352. [PubMed: 6158890]

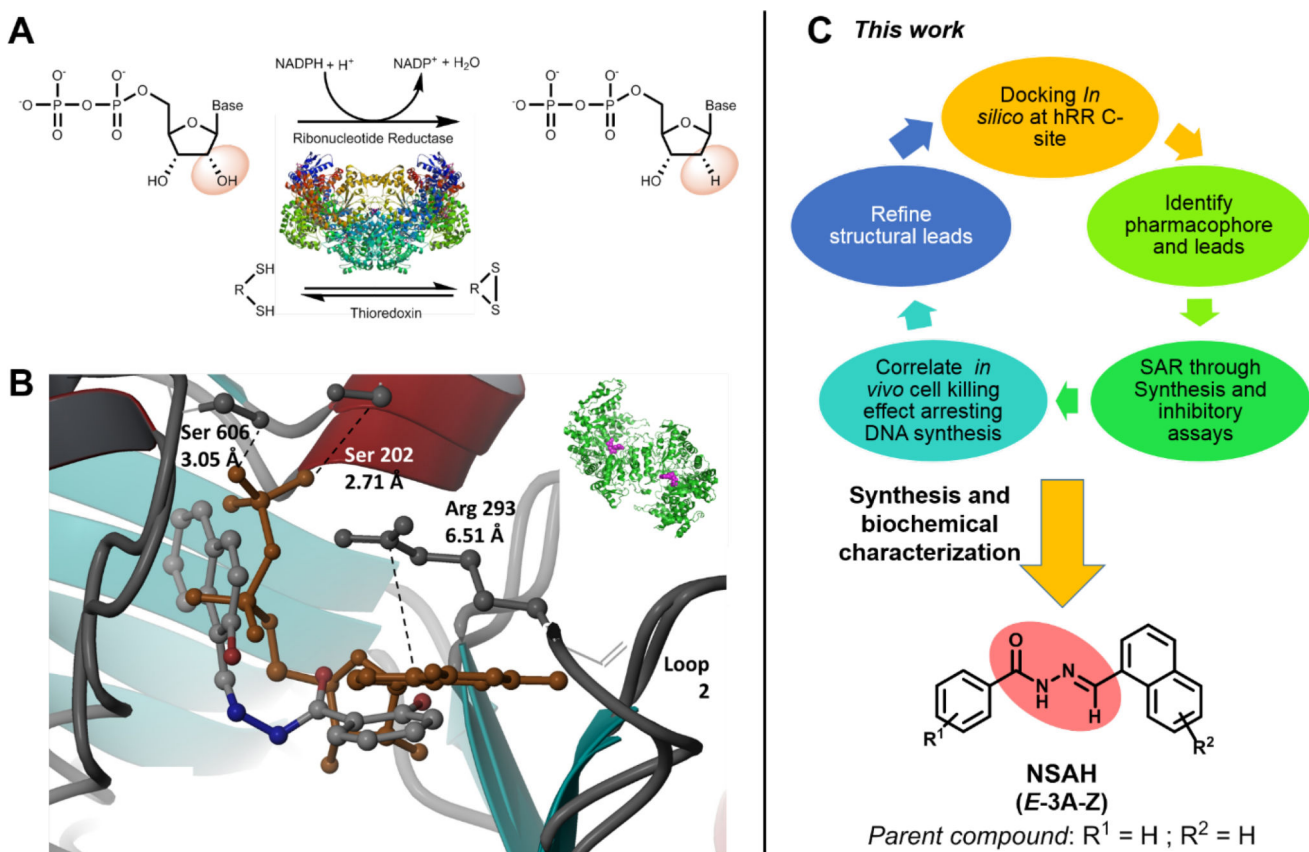


Figure 1.

A. Conversion of ribonucleoside diphosphates into deoxyribonucleoside diphosphates by RR and its redox coupled activity with thioredoxin; **B.** Comparison of lead compound Naphthyl Salicyl Acyl Hydrazone (NSAH or E-3a) and natural substrate GDP bound to the C-site of hRR (PDB ID: 5TUS)¹⁰; **C.** Overall approach leading to identification of novel hRR inhibitor whose analogs (E-3a-z) are synthesized and biochemically characterized in this report.

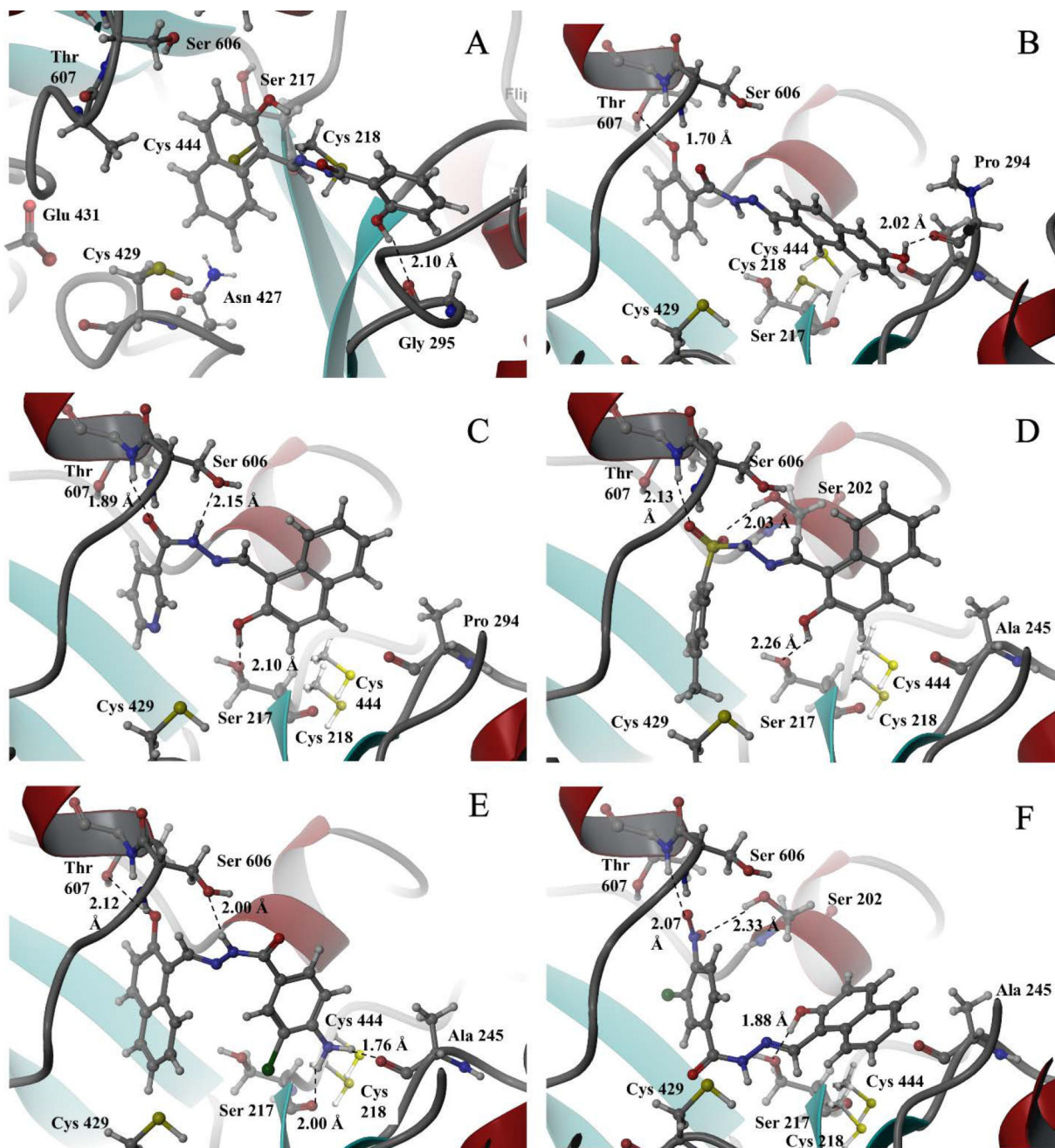


Figure 2.
 Predicted binding interactions for top-ranked NSAH candidates at the C-site of hRR based on the X-ray recently published structure PDB ID: 5TUS.¹⁰ A. *E-3a*; B. *E-3c*; C. *E-3f*; D. *E-3s*; E. *E-3t*; F. *E-3u*.

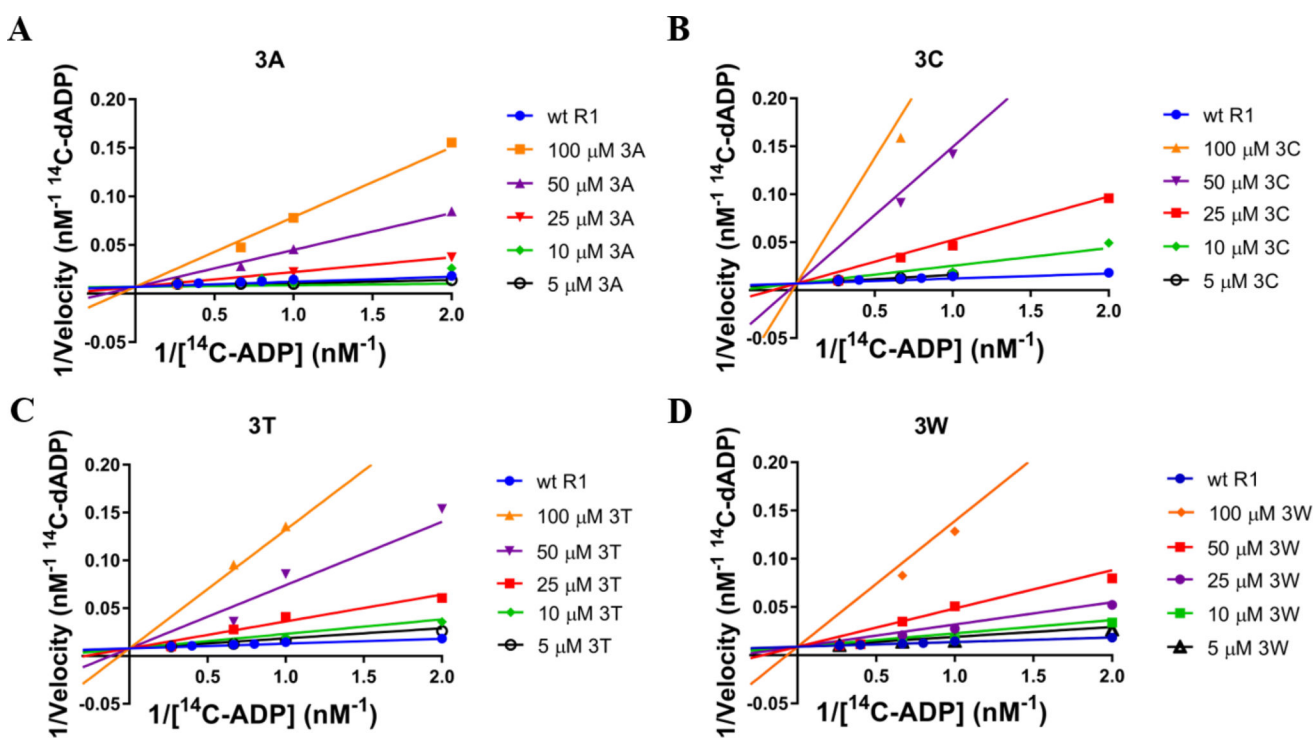


Figure 3.

A. Double-reciprocal plot for *E-3a*. All data sets converge upon a common y- intercept, supporting a competitive mechanism of inhibition. **B.** Double-reciprocal plot for *E-3c* also follows a competitive model. **C.** Double-reciprocal plot for *E-3t*, depicting competitive inhibition. **D.** Double-reciprocal plot for *E-3w* supports a competitive model of inhibition.

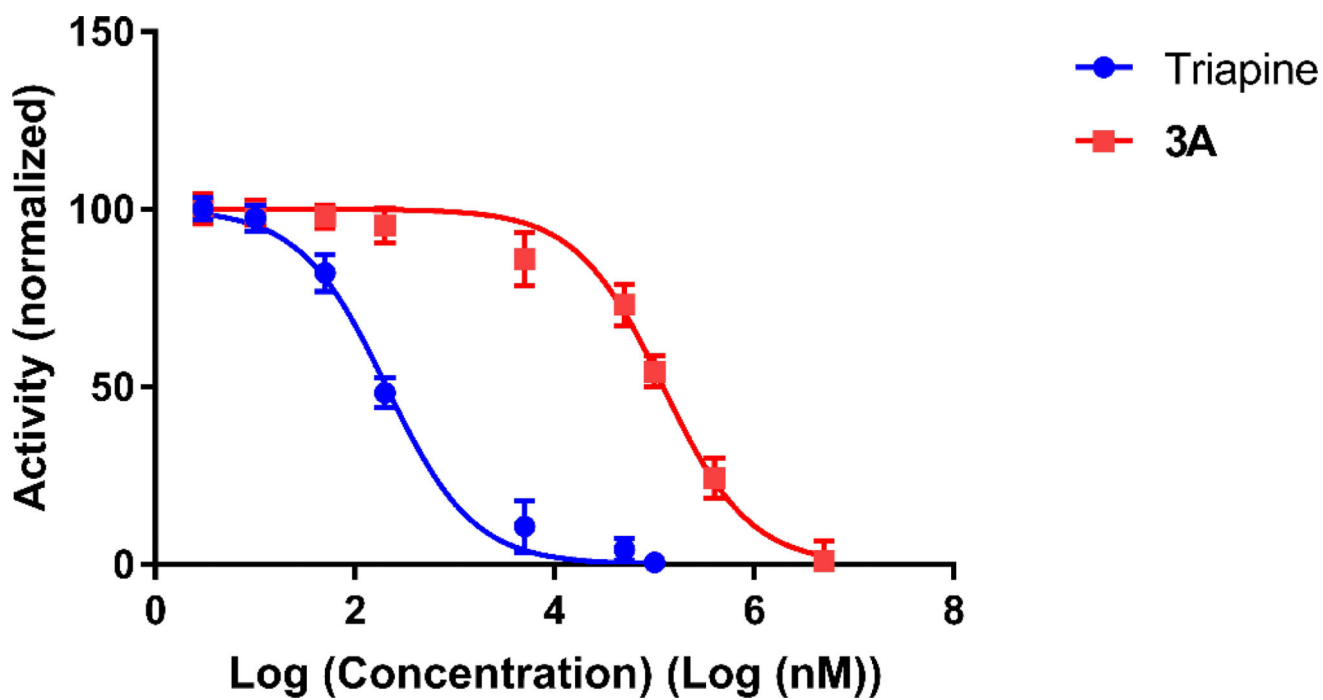


Figure 4. Sigmoidal dose-response curves for triapine and *E-3a* against hRRM2. The IC₅₀ values of triapine and *E-3a* are 0.185 and 123 μM, respectively.

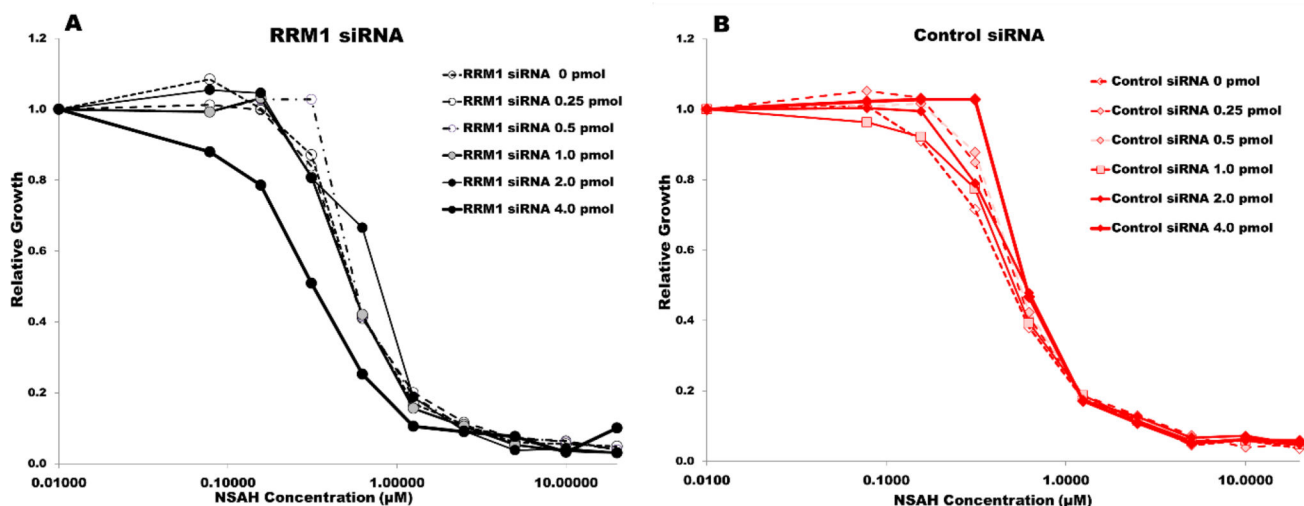
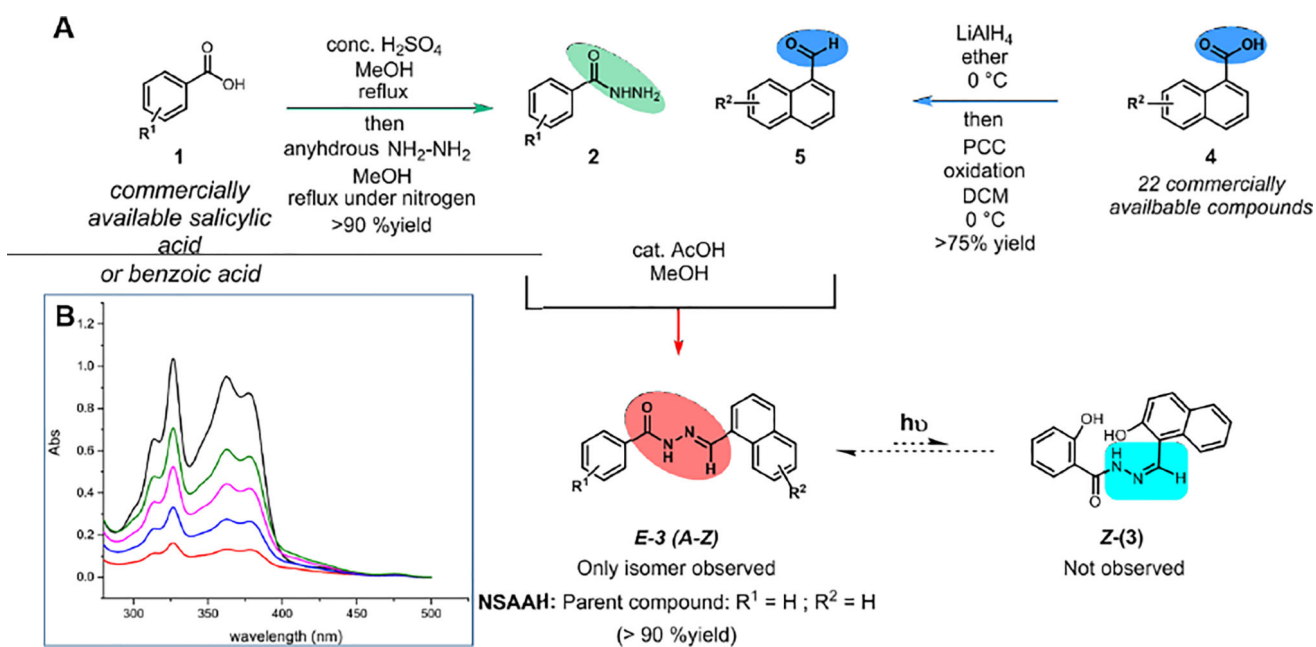


Figure 5.

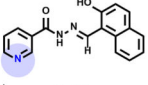
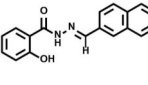
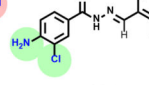
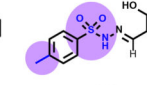
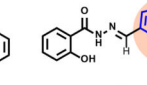
A and **B**. Sensitization of MDA-MB-231 cell line toward NSAH inhibitor under siRNA transfection and RRM1 knockdown conditions. **A**: Using RRM1 siRNA and **B**: Using Control-scrambled siRNA. Line displayed in **A** at the 4.0 pmol level represents the maximal sensitization occurring in the presence of *E-3a*, operating within an optimized siRNA concentration range.

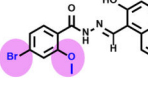
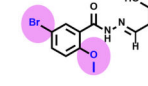
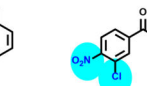
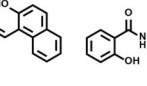
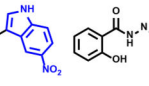
**Scheme 1.**

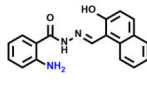
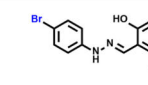
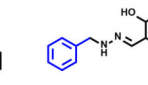
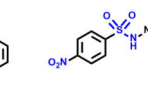
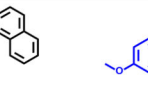
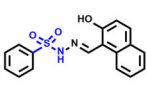
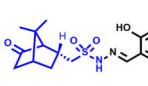
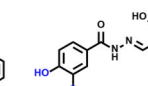
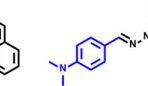
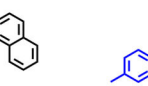
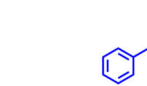
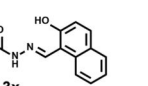
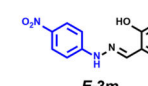

A. Modular synthesis of hRR inhibitor library.; Yields and other structural characterization per each analog is provided in the experimental section. Thermodynamic control of the condensation step leading to *E*-isomer is observed. **B.** UV profile for *E*-3a. λ_{max} at 320 nm is attributed to acyl hydrazone in *trans* configuration. The varying concentrations for *E*-3a are 2.0, 4.0, 8.0, 16.0 and 32.0 μ M respectively as measured in MeOH as a solvent. Data corrected for solvent and background.

Table 1

Structures, % yields, *in vitro* IC₅₀ values, and predicted solubility and permeability properties for *E-3a* and its analogs. Cellular IC₅₀ values are averaged from HCT116 and MDA-MB-231 cell lines. ClogP and membrane permeability parameters were predicted using Qikprop. Permeability is reported as a diffusion rate in nanometers/second. Other related properties are provided in Table S2 (SI).

A					
Analog					
IC ₅₀ against hRR	5.3 ± 1.8 μM	7.3 ± 1.5 μM	6.1 ± 1.7 μM	6.8 ± 1.5 μM	10.19 ± 2.1 μM
% yield from hydrazide	82 %	72 %	74 %	51 %	15 %
ClogP (octanol/water)	2.758	3.485	3.145	3.248	3.788
Permeability (nm/s)					
Caco-2	552	333	346	605	685
MDCK	260	150	358	288	329
Alteration from 3A	pyridyl	C6-hydroxyl	p-amino m-chloro	p-methyl sulfonyl	7-methyl indolyl

B					
Analog					
IC ₅₀ against hRR	13.56 ± 1.9 μM	16.63 ± 2.3 μM	16.65 ± 1.8 μM	20.7 ± 1.9 μM	21.14 ± 2.4 μM
% yield from hydrazide	85 %	85 %	63 %	85 %	64 %
ClogP (octanol/water)	4.362	4.216	3.428	2.742	2.629
Permeability (nm/s)					
Caco-2	1061	1053	137	62	171
MDCK	1392	1392	118	24	73
Alteration from 3A	p-bromo o-methoxy	m-bromo o-methoxy	m-bromo o-methoxy	5-nitro indolyl	5-hydroxy indolyl

C					
					
<i>E-3e</i> IC ₅₀ = 23.8 ± 2.3 μM	<i>E-3l</i> IC ₅₀ = 21.5 ± 3.6 μM	<i>E-3k</i> IC ₅₀ = 39.42 ± 2.7 μM	<i>E-3q</i> IC ₅₀ = 43.65 ± 3.1 μM	<i>E-3i</i> IC ₅₀ = 94.11 ± 3.9 μM	
					
<i>E-3o</i> IC ₅₀ = 121.8 ± 4.0 μM	<i>E-3r</i> IC ₅₀ = 297.7 ± 4.3 μM	<i>E-3g</i> IC ₅₀ = 686.8 ± 5.2 μM	<i>E-3h</i> IC ₅₀ = 95.2 ± 6.1 μM	<i>E-3j</i> IC ₅₀ = 86.83 ± 9.4 μM	
					
<i>E-3p</i> IC ₅₀ = 120.3 μM	<i>E-3m</i> IC ₅₀ = 70.1 μM	<i>E-3n</i> IC ₅₀ = 70.1 μM		<i>E-3a</i> IC ₅₀ = 130.7 μM	